Thesis for the degree of Licentiate of Engineering

Multidimensional Modulation Formats for Coherent Optical Communication Systems

Tobias A. Eriksson

CHALMERS

Photonics Laboratory
Department of Microtechnology and Nanoscience (MC2)
Chalmers University of Technology
Göteborg, Sweden, 2014

Multidimensional Modulation Formats for Coherent Optical Communication Systems

Tobias A. Eriksson

Göteborg, March 2014

Technical Report MC2-274
ISSN 1652-0769

Chalmers University of Technology
Department of Microtechnology and Nanoscience (MC2)
Photonics Laboratory, SE-412 96 Göteborg, Sweden
Phone: +46 (0) 31 772 1000

Printed by Chalmers reproservice, Chalmers University of Technology
Göteborg, Sweden, March, 2014

Multidimensional Modulation Formats for Coherent Optical Communication Systems

Tobias A. Eriksson
Photonics Laboratory, Department of Microtechnology and Nanoscience
Chalmers University of Technology, SE-412 96 Göteborg, Sweden

Abstract

Coherent optical receivers have enabled the use of multilevel modulation formats with high spectral efficiencies and long transmission reaches. Traditionally, modulation formats utilizing the two dimensions spanned by the amplitude and the phase of the signal have been dominating. This thesis is devoted to novel modulation formats exploring the possibilities of modulation formats in higher dimensional signal spaces to find formats with a good tradeoff between spectral efficiency and sensitivity.

The work included in this thesis can be divided into two parts, experimental and theoretical. The first part includes experimental demonstrations of several four- and eight-dimensional modulation formats where the sensitivity as well as the performance in terms of transmission reach is evaluated and compared to conventional modulation formats. 128-level set-partitioning QAM (128-SP-QAM) is demonstrated with 50 % increased transmission distance over polarization-multiplexed 16-ary quadrature amplitude modulation (PM-16QAM). Binary pulse position modulation in combination with QPSK (2PPM-QPSK) is shown to achieve 40 % increased transmission reach over PM-QPSK. Further, the eight-dimensional modulation format frequency and polarization switched QPSK (4FPS-QPSK) is shown to have 84 % increased transmission reach over polarization-multiplexed quadrature phase-shift keying (PM-QPSK) in a dual-carrier setup.

The second part includes theoretical work where the spectral efficiency and asymptotic power efficiency is evaluated for modulation formats in high dimensional signal spaces. The high dimensionality is achieved by considering multidimensional position modulation, which is a generalization of pulse position modulation, in combination with QPSK and polarization-switched QPSK. The different dimensions can be achieved by time slots, polarizations, frequency slots, modes of multimode fibers or cores of a multicore fiber.

Keywords: Fiber-optical communication, coherent detection, spectral efficiency, power efficiency, quadrature phase shift keying (QPSK), polarization-switched quadrature phase shift keying (PS-QPSK),16-ary quadrature amplitude modulation (16QAM), 128-level set-partitioning QAM (128-SP-QAM), binary pulse position modulation QPSK, multidimensional position modulation.

List of Papers

This thesis is based on the following appended papers:

[A] **T. A. Eriksson**, M. Sjödin, P. Johannisson, P. A. Andrekson, and M. Karlsson, "Comparison of 128-SP-QAM and PM-16QAM in Long-haul WDM Transmission," *Optics Express*, vol. 21, no. 16, pp. 19269-19279, 2013.

[B] **T. A. Eriksson**, M. Sjödin, P. Johannisson, E. Agrell, P. A. Andrekson, and M. Karlsson, "Frequency and Polarization Switched QPSK," *European Conference and Exhibition on Optical Communication (ECOC)*, London, England, paper Th.2.D.4, 2013.

[C] M. Sjödin, **T. A. Eriksson**, P. A. Andrekson, and M. Karlsson, "Long-Haul Transmission of PM-2PPM-QPSK at 42.8 Gbit/s," *Optical Fiber Communication Conference (OFC)*, Anaheim, USA, paper OTu2B.7, 2013.

[D] **T. A. Eriksson**, P. Johannisson, B. J. Puttnam, E. Agrell, P. A. Andrekson, and M. Karlsson, "K-over-L Multidimensional Position Modulation," Submitted to *IEEE Journal of Lightwave Technology*, September 2013; revised, January 2014.

Related publications and conference contributions by the author, not included in the thesis:

[E] **T. A. Eriksson**, M. Sjödin, P. A. Andrekson, and M. Karlsson, "Experimental Demonstration of 128-SP-QAM in Uncompensated Long-Haul Transmission," *Optical Fiber Communication Conference (OFC) 2013*, Anaheim, USA, paper OTu3B.2, 2013.

[F] J. Li, E. Tipsuwannakul, **T. A. Eriksson**, M. Karlsson, and P. A. Andrekson, "Approaching Nyquist Limit in WDM Systems by Low-Complexity Receiver-Side Duobinary Shaping," *IEEE Journal of Lightwave Technology*, vol. 30, no. 11, pp. 1664-1676 , 2012.

[G] E. Tipsuwannakul, J. Li, **T. A. Eriksson**, M. Karlsson, and P. A. Andrekson, "Transmission of 3×224 Gbit/s DP-16QAM Signals with (up to) 7.2 bit/s/Hz Spectral Efficiency in SMF-EDFA Links," *Optical Fiber Communication Conference (OFC) 2012*, Los Angeles, USA, paper OW4C.6, 2012.

[H] E. Tipsuwannakul, J. Li, **T. A. Eriksson**, F. Sjöström, J. Pejnefors, P. A. Andrekson, and M. Karlsson, "Mitigation of Fiber Bragg Grating-Induced Group-Delay Ripple in 112 Gbit/s DP-QPSK Coherent Systems," *Optical Fiber Communication Conference (OFC) 2012*, Los Angeles, USA, paper JW2A.69, 2012.

[I] **T. A. Eriksson**, E. Tipsuwannakul, J. Li, M. Karlsson, and P. A. Andrekson, "625 Gbit/s Superchannel Consisting of Interleaved DP-16QAM and DP-QPSK with 4.17 bit/s/Hz Spectral Efficiency," *European Conference and Exhibition on Optical Communication (ECOC) 2012*, Amsterdam , Netherlands, paper P4.11, 2012.

[J] E. Tipsuwannakul, J. Li, **T. A. Eriksson**, L. Egnell, F. Sjöström, J. Pejnefors, P. A. Andrekson, and M. Karlsson, "Influence of Fiber-Bragg Grating-Induced Group-Delay Ripple in High-Speed Transmission Systems," *Journal of Optical Communications and Networking*, vol. 4, no. 6, pp. 514-521 , 2012.

Acknowledgement

The work leading up to this licentiate thesis could not have been completed without the help and support of the many great coworkers at the photonics laboratory.

To start with, I would like to thank my supervisors Prof. Peter Andrekson and Prof. Magnus Karlsson for giving me the opportunity to start as a Ph.D. student in the fiber group and for all their support.

My supervisor Docent Pontus Johannisson deserves my deepest thanks, he has been one of the most important persons for me during the time I spent in the fiber group so far. I dream of one day having a BBQ-party on Pontus newly pressure-washed porch.

I would like to thank my supervisor Prof. Erik Agrell for giving me a different view of many things and for being the sharpest proofreader to walk this earth.

I would like to thank Ekawit Tipsuwannakul for introducing me to the research field of fiber optical communications during the time he was supervising me as a master thesis student. Before meeting him I had no thoughts on pursuing a Ph.D. degree. Martin Sjödin deserves my thanks for our collaboration and for his guidance when I started in the fiber group. Also for our many pingpong matches and duets in the lab. The imperial stout that I have brewed for the licentiate party is dedicated to him.

The two great office mates that I have had deserves my gratitude; Yuxin Song, thanks for all the pingpong and for always highlighting the next astronomical event. Henrik Eliasson, for being such a nice beer brewing buddy and enduring my sporadic singing in the office.

Further the following people deserves my thanks. Calle Lundström for our fruit moments and his proofreading skills, Jianqiang Li for our collaboration in the lab, Samuel Olsson for our pingpong games and for our sourdough discussions, Ben Kögel for all the football, brewing and setting the lunch standards, Abel Lorences Riesgo for being there for me when I need to talk football and for our visit to Anfield with Henrik, Jörgen Bengtsson for joining in welcoming me and preventing work from being the lunch topic, Clemens Krückel for his magician appreciation, Aleš Kumpera for showing me that beer is an appropriate drink to fika, Bill Corcoran for BBQing in shorts in January, Martin Stattin for showing me how to stand like a guy and Ben Puttnam for our long-distance collaboration.

A big thanks to the rest of the people that are or has been with the Photonics Laboratory during my time here so far, you all make this a great place to work at!

Finally, to Karin for being the best and for your love. Without you this thesis would never have been possible.

Tobias A. Eriksson

Göteborg
March 2014

List of Acronyms

KPPM K-ary PPM (35)
128-SP-QAM 128-level set-partitioning QAM (4, 23, 28–30, 37–39, 47, 49–52, 54)
16PPM 16-ary PPM (35)
16QAM 16-ary quadrature amplitude modulation (21, 43, 51, 52, 54)
2D two-dimensional (19, 22, 24, 26, 31)
2PPM binary pulse position modulation (32)
2PPM-QPSK binary pulse position modulation QPSK (27, 28, 38, 48)
32-SP-QAM 32-level set-partitioning QAM (23, 28, 30, 39)
4D four-dimensional (16, 22–24, 30, 31, 39)
4FPS-QPSK 4-ary frequency and polarization switched QPSK (5, 39, 47–49, 51)
4PAM 4-ary pulse amplitude modulation (16, 21)
4iMDPM-QPSK 4-ary inverse multidimensional position modulation QPSK (5, 36)
512-SP-QAM 512-ary set-partitioning QAM (30)
6polSK-QPSK 6-level polarization shift keyed QPSK (23, 30, 31)
8-QAM 8-ary quadrature amplitude modulation (29, 30)
8D eight-dimensional (31, 36)
8iMDPM-QPSK 8-ary inverse multidimensional position modulation QPSK (5, 36, 37)
ADC analog-to-digital converter (3, 12, 13, 42, 44)
APE asymptotic power efficiency (18, 20, 21, 23, 27–31, 35–37)
ASE amplified spontaneous emission (8–10)
AWGN additive white Gaussian noise (8, 16, 18, 46, 51)
B2B back-to-back (30)
BER bit-error probability (17, 18)
BPSK binary phase-shift keying (10, 15, 18, 20, 21, 31, 36)
CMA constant modulus algorithm (47–50, 54)

DCF dispersion compensating fiber (3, 9, 44)
DD-LMS decision-directed least mean square (49)
DSP digital signal processing (9, 11, 15, 16, 19, 20, 22, 24, 41, 43, 44, 54)
EDC electronic dispersion compensation (44, 46)
EDFA Erbium doped fiber amplifier (3, 7–9, 11, 15, 44, 53)
ENOB effective number of bits (13)
ETDM electrical time-division multiplexing (15)
FEC forward error correction (29, 37, 54)
FFT fast Fourier transform (50)
FIR finite impulse response (45, 46)
FSK frequency shift keying (32)
FWM four-wave mixing (3)
I/Q-modulator in-phase and quadrature-modulator (25, 28)
IF intermediate frequency (42, 43, 50)
iMDPM inverse-MDPM (36)
ISI intersymbol interference (44, 46)
LDPC low-density parity check (29, 30, 54)
LO local oscillator (10, 11, 41, 43, 50, 51)
MDPM multidimensional position modulation (36, 37)
MIMO multiple input multiple output (53)
MPPM multi-pulse position modulation (35, 36)
MZM Mach-Zehnder modulator (20, 22, 25, 28, 32)
OFDM orthogonal frequency division multiplexing (30)
OOK on-off keying (10, 15, 19)
OSNR optical signal-to-noise ratio (4, 5, 10, 30)
OTDM optical time-division multiplexing (15)
PBC polarization beam combiner (20, 25)
PM-16QAM polarization-multiplexed 16QAM (4, 16, 21–23, 28–30, 37, 38, 47, 49–52, 54)
PM-64QAM polarization-multiplexed 64-ary quadrature amplitude modulation (30)
PM-BPSK polarization-multiplexed BPSK (20)
PM-QPSK polarization-multiplexed QPSK (4, 5, 16, 18–20, 24–26, 28–31, 35–39, 47, 48, 50, 54)
PMD polarization mode dispersion (46)
POLQAM polarization-QAM (23)
PPM pulse position modulation (26, 28, 35–37)
PS-CMA polarization-switched CMA (47, 48)
PS-QPSK polarization-switched QPSK (5, 23–27, 31, 32, 35–38, 47, 50, 51, 54)

PSK phase shift keying (18, 51)
QAM quadrature amplitude modulation (18, 23)
QPSK quadrature phase-shift keying (4, 5, 16–18, 20, 22–26, 28, 30, 31, 35–37, 42, 43, 47, 50–52, 54)
RF radio frequency (13, 21, 41)
SE spectral efficiency (4, 5, 16, 18, 20, 21, 23, 27–30, 35–39, 48)
SER symbol error probability (30, 31)
SMF standard monomode fiber (44)
SNR signal-to-noise ratio (4, 17, 18, 51)
SO-PM-QPSK subset-optimized PM-QPSK (31)
SOP state-of-polarization (23, 30)
SP set-partitioning (23, 29)
WDM wavelength division multiplexing (3, 9, 15, 25, 29, 36, 38, 44, 53)
XOR exclusive or (25, 29)

Table of Contents

Chapter 1

Introduction

The global communication network, including all types of data transmission such as telephone and the Internet is ever evolving. Today, streaming high-definition movies or live sport are almost taken for granted while just a few years ago this would have seemed impossible. In the near future, streaming services using so called *4K resolution* [1] and *8K resolution* [2] is expected to emerge, where the latter standard has 16 times as many pixels compared to what is today considered high-definition. Further, cloud computing services are starting to become more popular [3] and online gaming (including cloud gaming), video chats, social networks, blogs, file sharing, etc. are ever so popular. The demand for high-bandwidth services like these, together with the increasing number of Internet users, see Fig. 1.1, sets a huge requirement on the architecture and data-capacity of the supporting technologies. In Fig. 1.1, it is clear that in the next year or two, half of the population of the world will have Internet access and in the same time frame the percentage of Europe's population that have access to the Internet will reach 80 % [4, 5]. Much of this development has been enabled by fiber optical communication systems which forms the backbone of both the Internet and the mobile telephone network. To keep up with the increasing demand for bandwidth, which seems to see no saturation in the coming years, a lot of research is needed in all areas related to fiber optical transmission.

1.1 A Brief History of Fiber Optical Communication

Fiber optical communication systems were basically enabled by two crucial inventions, the laser and the optical fiber. The laser evolved from the first

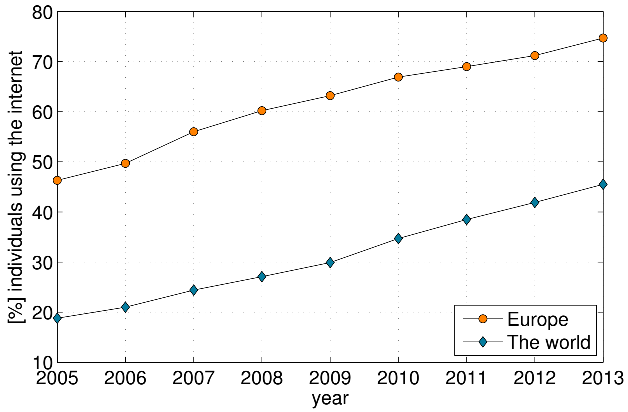

Figure 1.1: Percentage of individuals using the Internet in Europe and the world, data from [4, 5].

demonstration of stimulated emission in a ruby crystal by Maiman in 1960 [6], with an important milestone being the invention of the semiconductor laser in 1962 [7, 8]. In 1966, Kao and Hockham proposed that optical fibers could be fabricated with low loss using silica glass [9] and in 1970 the first single-mode fiber was constructed with 20 dB/km of loss at 633 nm [10]. Three years later the loss was down to 4 dB/km (although being in a multimode fiber) [11] and in 1976 a loss of 0.47 dB/km was demonstrated [12]. The loss in optical fibers has since then been improving with the current record being as low as 0.148 dB/km at 1570 nm [13] and 0.149 dB/km at 1550 nm [14]. Other milestones during the 1960-1970's include fundamental work on optical receivers [15], the introduction of the first commercial continuous semiconductor laser that could operate continuously at room temperature [16, Appendix B] and the discovery of the transmission window in optical fibers around 1550 nm [17]. Further, the zero-dispersion wavelength at 1300 nm was pointed out in 1975 [18].

An important milestone was the fiber optical system test that was performed by Bell Labs in 1976, and is known as *the Atlanta Experiment*, where transmission over buried fibers was demonstrated at a bitrate of 44.7 Mbit/s [19]. Following this successful demonstration was a plethora of field trials in Europe, North America and Japan [20]. The first commercial fiber optical transmission system was deployed by GTE Laboratories between Long Beach and Artesia in California with the system up and running in April 1977. This system was 10 km long and carried telephone traffic at 6.3 Mbit/s [16, Chapter 14]. GTE Laboratories had been racing against AT&T who only six weeks later had their system, deployed in Chicago, up and running [16, Chapter 14]. However, it should be mentioned that the AT&T system was first in terms of sending test signals.

During the 1980's, telecom companies started to deploy optical fiber systems in which conventional single-mode fibers was typically used and the operating wavelength was either 1300 nm or 1550 nm [16, 20]. In 1988 the first transatlantic cable that was using fibers, TAT-8, were completed, despite the original problems with shark attacks on the fiber cable [21]. TAT-8 used signal lasers at 1310 nm utilizing the low dispersion at that wavelength and had two fiber pairs installed which each could transmit 280 Mbit/s [22]. The first transpacific fiber optical cable, TPC-3, was installed one year after TAT-8 [22].

The Erbium doped fiber amplifier (EDFA) was invented in the mid 1980 [23–25] and revolutionized the fiber-optical communication industry. Suddenly, it was possible to amplify the signal in the optical domain and the use of repeaters which detected and retransmitted the signal could be abandoned. The EDFA opened the way for wavelength division multiplexing (WDM) since many wavelength channels could be amplified simultaneously compared to the old repeater technology where each WDM-channel had to be retransmitted individually. In 1990, a four-channel WDM system using EDFAs, where each channel carried 2.4 Gbit/s, was demonstrated [26].

Chromatic dispersion was always a limiting problem which had been solved by operating in the low dispersion region around 1300 nm or by using dispersion-shifted fibers, as in for instance [27] where 2.4 Gbit/s transmission over 21,000 km was achieved. However, it was soon recognized that four-wave mixing (FWM) heavily distorts the signals in a WDM system when operating in the low-dispersion regime [28]. In 1993, it was realized that the nonlinear effects could be suppressed by avoiding non-zero dispersion and the first dispersion-managed link was demonstrated using dispersion-shifted fibers in combination with conventional single-mode fibers [29]. The dispersion compensating fiber (DCF) was introduced in the mid 1990's [30, 31], employing large dispersion with opposite sign compared to the conventional single-mode fiber. (This idea was however much older [32]). The use of DCFs to periodically compensate for the dispersion opened up possibilities for long-haul WDM transmission such as 16 WDM-channels each carrying 10 Gbit/s over 1000 km in 1995 [33] as well as one of the first Tbit/s systems demonstrated in 1996 using 55 WDM channels [34].

Another milestone in the fiber optical community was when analog-to-digital converters (ADCs) and electronics with sufficient speed enabled real-time coherent receivers utilizing digital signal processing to perform phase-tracking so that free-running local-oscillators could be used [35, 36]. The coherent receiver, which is discussed in Chapter 3, gives access to the full optical field enabling multi-level modulation formats with unconstrained choices

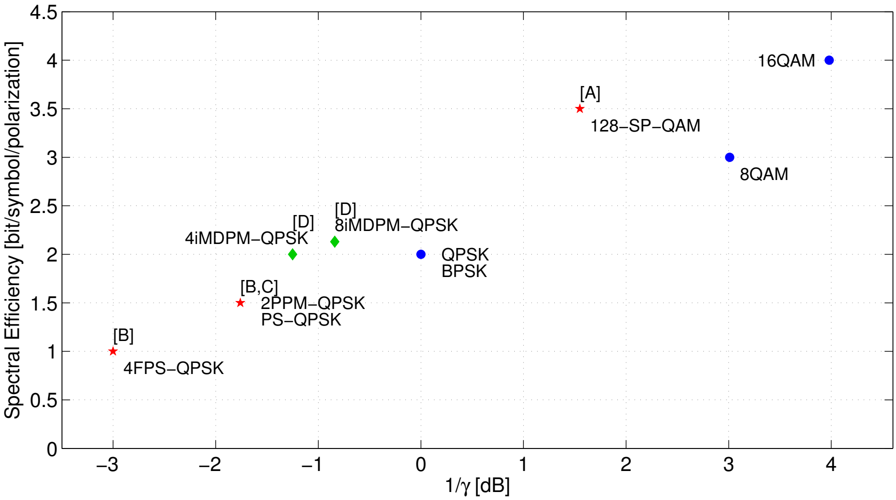

Figure 1.2: Spectral efficiency as a function of asymptotic power efficiency penalty for some conventional modulation formats (blue circles), the modulation formats that have been experimentally investigated in paper A-C (red stars) and two formats from the theoretical study in paper D (green diamonds).

of phase and amplitude. The fiber optical communication systems discussed in this thesis are based on coherent detection.

1.2 Motivation for This Thesis

In coherent optical communication systems, polarization-multiplexed QPSK (PM-QPSK) is the dominating modulation format for long-haul systems and polarization-multiplexed 16QAM (PM-16QAM) is considered the modulation format to be used when higher spectral efficiency (SE) is required. The step between these two formats is huge in terms of required optical signal-to-noise ratio (OSNR) which translates into much shorter transmission reach for PM-16QAM. In paper A, 128-level set-partitioning QAM (128-SP-QAM) is experimentally investigated. This format offers a step in between PM-QPSK and PM-16QAM in terms of sensitivity with just a small sacrifice in SE. This is illustrated in Fig. 1.2 where the SE for different formats is plotted as a function of asymptotic power efficiency penalty, which gives the sensitivity penalty over quadrature phase-shift keying (QPSK) for asymptotically high signal-to-noise ratio (SNR).

On the other hand, for transmission links where the available OSNR is not high enough to support PM-QPSK, other formats have to be considered such as those illustrated in Fig. 1.2. In paper B, both polarization-switched QPSK (PS-QPSK) and 4-ary frequency and polarization switched QPSK (4FPS-QPSK) are experimentally investigated. PS-QPSK offers a 1.76 dB better power efficiency than QPSK at the loss of 0.5 bit/symbol/polarization in SE. In paper C, a different implementation of PS-QPSK is experimentally investigated where binary pulse position modulation is used instead of polarization switching. If even higher sensitivities are required, 4FPS-QPSK can be used which has half the SE compared to QPSK but 3 dB increased power efficiency.

In the theoretical and numerical investigations in paper D, whole families of modulation formats based on multidimensional position modulation, which is a generalization of pulse position modulation, are introduced. Two formats from that study are highlighted in Fig. 1.2, namely the 8-dimensional format 4-ary inverse multidimensional position modulation QPSK (4iMDPM-QPSK) and the 16-dimensional format 8-ary inverse multidimensional position modulation QPSK (8iMDPM-QPSK). As seen these two formats offer increased power efficiency compared to QPSK without any loss in SE.

Chapter 2

Basics of Coherent Fiber Optical Communication

This chapter is divided into two parts where the first part introduces some basic knowledge of the fiber optical communication channel followed by the second part which discusses the coherent optical detection technique. It should be mentioned that the following sections only gives a brief overview.

2.1 The Fiber Optical Channel

This section introduces some basic concepts of a fiber optical communication system starting with the key components followed by a description of the additive white Gaussian noise channel model. After that dispersion is introduced followed by a model for nonlinear distortion.

2.1.1 Basic Fiber Optical Communication System

The optical fiber works on the principle of *total internal reflection* and is made out of silica glass. The optical fiber has a loss of around 0.2 dB/km at a wavelength of 1550 nm. For long-haul optical systems typically span lengths of 50-120 km of fiber are used where the optical signal is amplified after each span, as illustrated in Fig. 2.1 [37, Chapter 2].

Typically, the amplifiers that are used are EDFAs however other amplification technologies exist such as Raman amplifiers [38], semiconductor optical amplifiers [39] and phase-sensitive fiber amplifiers [40]. The operating principle of an EDFA is that the fiber is doped with the rare-earth element Erbium

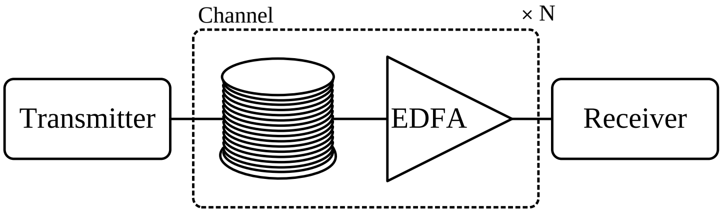

Figure 2.1: Basic outline of a fiber optical communication systems showing the transmitter, the transmission link consisting of N fiber spans and amplifiers, and the receiver.

which can be optically pumped to achieve population inversion and therefore optical gain. As any other amplifier, the EDFA adds noise. The noise originates from the spontaneously emitted photons from the exited Erbium ions. These photons will have random wavelength, phase and polarization and will experience gain as they propagate in the EDFA. Hence, the noise generated in the EDFA is called amplified spontaneous emission (ASE) noise.

The EDFA typically have a gain in the region of 1530–1565 nm which is called the C-band and the gain can be extended to the O-band (1260–1360 nm), E-band (1360–1460 nm), S-band (1460–1530 nm), L-band (1565–1625 nm) and the U-band (1625–1675 nm) [41].

2.1.2 Additive White Gaussian Noise Channel

The simplest model of a fiber optical link is to consider only additive white Gaussian noise (AWGN) as is shown in Fig. 2.2. Note that the input and output of the link are discrete while the channel itself is continuous time. The added noise n_k is zero-mean Gaussian with noise variance σ^2, i.e. $n_k \sim \mathcal{N}(0, \sigma^2)$ [42, Section 3.3.4]. As seen the whole link (channel) with EDFAs and fiber spans in Fig. 2.1 are replaced by the added noise n_k. The noise variance σ^2 will depend on the link parameters such as span loss and EDFA noise figure. Note that in fiber optical communication systems, matched-filtering [43, p. 178–182] is typically not applied. Instead a suboptimal low-pass filter, often induced by the limited bandwidth of the receiver, is used. The AWGN channel is a good approximation when the optical power launched into each span is low. However, when the optical power is high the channel becomes nonlinear and the AWGN channel model is no longer a good approximation.

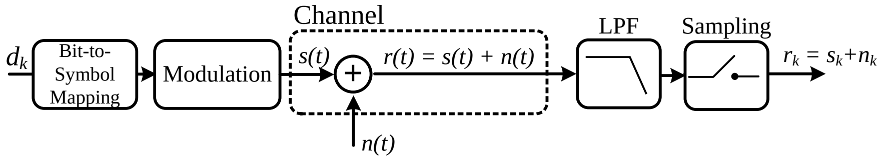

Figure 2.2: The AWGN channel model. The discrete bit sequence d_k is mapped to symbols that are modulated onto the optical carrier. The signal is transmitted over the optical link where the impairments are modeled as AWGN. The received signal is low-pass filtered (LPF) and sampled and the output r_k is a discrete set of samples.

2.1.3 Dispersion

The different frequency components of a pulse propagating in an optical fiber will have different group velocities. The result of this is that pulses will be broadened during propagation. This effect is typically called *group velocity dispersion* or sometimes referred to as just *dispersion*. This effect can be mitigated in different ways such as inline compensation where each span is followed by a dispersion compensating module based on DCF or chirped fiber-Bragg gratings. Alternatively, electronic dispersion compensation can be used where all the accumulated dispersion in the link is mitigated in the digital signal processing (DSP) domain. Dispersion compensation is discussed in section 4.3.

2.1.4 Nonlinear Transmission Impairments

Together with the noise added by the EDFAs in a link, the nonlinear distortions are the limiting factors for a fiber optical transmission system. The nonlinear effects arise from the *Kerr effect* and the fact that the core of the optical fiber is small which gives high field intensity. The types of nonlinear distortion that will arise are dependent on the system and will be very different depending on if inline dispersion compensation is used or not, if the system is single channel or a WDM system, the symbol rate and the modulation format that is transmitted. Typically, there exists an optimal launch power into the fiber spans as qualitatively illustrated in Fig. 2.3 where in the low launch power region the system is limited by the ASE noise generated in the EDFAs and in the high launch power region the system is limited by the nonlinear distortions.

The long-haul fiber optical systems that have been experimentally implemented in this thesis are not using any inline dispersion compensation and all the accumulated dispersion is compensated for in the DSP. For these types of systems, the recently developed *Gaussian noise model* [44–46] has been

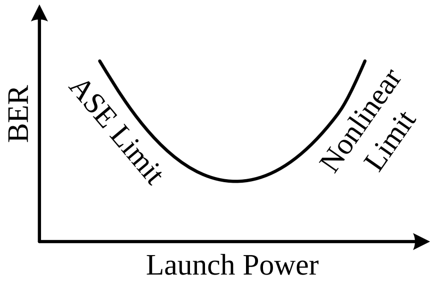

Figure 2.3: Typical behavior of a fiber optical link showing that there exists an optimal launch power and that for low launch power the system is limited by ASE noise and for high launch power the system is limited by nonlinear distortions.

shown to approximate the channel with good agreement. With this model, the nonlinear distortions are approximated as Gaussian and simply degrades the OSNR as

$$\mathrm{OSNR} = \frac{P_{\mathrm{sig}}}{P_{\mathrm{ASE}} + P_{\mathrm{NLI}}}, \tag{2.1}$$

where P_{sig} is the signal power, P_{ASE} is the ASE noise power and P_{NLI} is the nonlinear interference power and is proportional to P_{sig}^3 [44–46]. Using this model, the system will again follow the behavior illustrated in Fig. 2.3.

2.2 Coherent Detection

In fiber optical communication systems, there are two methods for detecting the optical signal. The first one is *direct detection* where a photo-detector is used to generate a current that is proportional to the optical power. This is the traditional method and is used for on-off keying (OOK). The photo-detector is a square-law detector, i.e. the output current is proportional to the power of the optical field. Thus, the phase of the optical signal is not detected. Using a *delay interferometer*, the relative phase between symbols can be detected using direct detection. This allows for direct detection of phase modulated formats such as binary phase-shift keying (BPSK), which has roughly 3 dB better sensitivity compared to OOK.

During the 1980's, a lot of research was focused on coherent detection systems due to the increased sensitivity over direct detection [23, 47, 48]. These coherent systems were hard to implement since they required an optical phase-locked loop to synchronize the local oscillator (LO) phase to the signal phase.

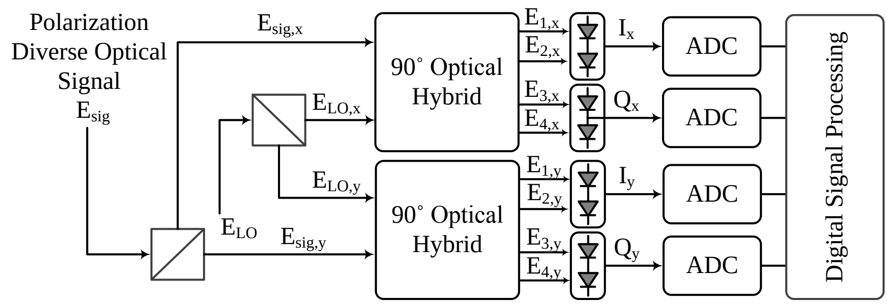

Figure 2.4: Schematics of the optical front-end of a polarization-diverse coherent receiver.

However, when the EDFA was invented [24, 25, 49], the receiver sensitivity could be significantly increased by optical pre-amplification and the interest in coherent detection was lost.

The interest in coherent detection was renewed when real-time measurements using coherent receivers with free-running LOs where demonstrated [36, 50, 51]. This time, the focus was on spectrally efficient modulation formats which were enabled due to the access to information of the full optical field with the coherent receiver. Further, the speed of electronics had reached a point where DSP could be used thus allowing compensation of signal distortions in the digital domain. Most importantly, the frequency- and phase-offset from the LO could be compensated in the digital domain, making the use of complicated hardware phase tracking unnecessary. The use of DSP also opened up a whole new research field on its own where dispersion compensation, nonlinear mitigation, equalization and polarization demultiplexing and tracking could be performed in the digital domain.

2.2.1 Coherent Optical Front-End

The optical front-end of a typical polarization-diverse coherent receiver is shown in 2.4. The electrical field of the LO is denoted E_{LO}. The signal and the LO are first split into two orthogonal polarization states, $E_{sig,x}, E_{sig,y}, E_{LO,x}$ and $E_{LO,y}$, by the polarization beam-splitters. The 90° optical hybrids have 4 outputs each and the working principle for one hybrid is illustrated in Fig. 2.5. The four outputs correspond to the two quadratures given in pairs, where the signals forming a pair have a 180° relative phase shift [52, 53]. The photo-current from each photo-detector after one optical hybrid, here shown for the x-polarization, is given by

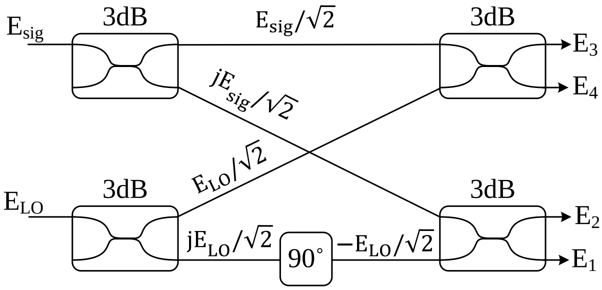

Figure 2.5: Principles of a 90° hybrid with 4 outputs.

$$\begin{bmatrix} i_{I+}(t) \\ i_{I-}(t) \\ i_{Q-}(t) \\ i_{Q+}(t) \end{bmatrix} \propto \begin{bmatrix} \frac{1}{2}\mathrm{Re}\{E_x(t)E_{LO,x}^*\} + \frac{1}{4}|E_x(t)|^2 + \frac{1}{4}|E_{LO,x}|^2 \\ -\frac{1}{2}\mathrm{Re}\{E_x(t)E_{LO,x}^*\} + \frac{1}{4}|E_x(t)|^2 + \frac{1}{4}|E_{LO,x}|^2 \\ \frac{1}{2}\mathrm{Im}\{E_x(t)E_{LO,x}^*\} + \frac{1}{4}|E_x(t)|^2 + \frac{1}{4}|E_{LO,x}|^2 \\ -\frac{1}{2}\mathrm{Im}\{E_x(t)E_{LO,x}^*\} + \frac{1}{4}|E_x(t)|^2 + \frac{1}{4}|E_{LO,x}|^2 \end{bmatrix}. \tag{2.2}$$

The photo-currents for the y-polarization is given in the same way, but replacing x with y. If balanced detection is used, such that $i_{xI}(t) = i_{xI+}(t) - i_{xI-}(t)$ and $i_{xQ}(t) = i_{xQ+}(t) - i_{xQ-}(t)$, the output signals will be

$$\begin{bmatrix} i_{Ix}(t) \\ i_{Qx}(t) \end{bmatrix} \propto \begin{bmatrix} \mathrm{Re}\left(E_x(t)E_{LO,x}^*\right) \\ \mathrm{Im}\left(E_x(t)E_{LO,x}^*\right) \end{bmatrix}. \tag{2.3}$$

The signals in the y-polarization are obtained in the same way, using a second 90° optical hybrid [54, p. 167–169]. In this way, both quadratures in the two polarizations can be detected. It should be noted that balanced detection is not required. With single-ended detection, optical hybrids without the extra 180° phase shifts are used and the photocurrent for one output will be $i_{xI}(t) = \mathrm{Re}\left(E_x(t)E_{LO}^*\right) + \frac{1}{2}|E_x(t)|^2 + \frac{1}{2}|E_{LO,x}|^2$. The drawback of this scheme is that the signal envelope is not removed, which results in that the power of the LO must be much larger than the signal power to make the coherent term dominate.

2.3 Analog-to-Digital Converters

The four output photocurrents from the optical hybrids are sampled using ADCs. The basic functionality of the ADC is to sample the signal in time with a fixed time-base, which converts the analog signal into a discrete-time signal. The ADC quantizes the signal into a finite set of values which is determined by the resolution [53]. The bandwidth and sampling rate of the ADCs are often stated as the bottle-neck in coherent fiber-optical communication systems and determines how high-bandwidth optical signals that can be detected with a single receiver. The amplitude resolution of the ADCs determines how many signaling-levels that can be used. A limiting factor for the resolution is timing jitter which reduces the effective number of bits (ENOB) [55]. To realize high-speed ADCs, time-interleaving of lower speed ADCs is often used and digital circuits perform the interleaving of the sampled signals and compensates for any mismatch between the different ADCs [56]. Alternatively, the time-interleaving can be performed in the optical domain where the optical signal is sampled using a short optical pulse [57, 58]. However, so far, this method is not commercially used and compared to the time-interleaving in the radio frequency (RF)-domain there are limitations such as that the relative phase between the LO and the signal is drifting in the different parallel sampling arms. Time-interleaving in the optical domain can be done with photonic integration which potentially can overcome the phase-drift issue and also provide lower timing-jitter compared to time-interleaved ADCs in the RF-domain [59, 60].

Chapter 3

Modulation Formats

In the past, OOK has been the dominating modulation format, mainly because it can be generated and detected with low complexity [61]. There was no need to use more advanced modulation formats since the throughput in a link could be increased by adding more WDM channels [62, 63] and using electrical time-division multiplexing (ETDM) [64, 65].

In the research community, optical time-division multiplexing (OTDM) was also a hot topic for increasing the throughput [66, 67]. Also, combing OTDM and WDM was investigated [68]. However, due to the complexity of multiplexing and demultiplexing OTDM, WDM emerged as the dominating technology in commercial systems. OOK can be detected without the need of any phase reference and the only competing modulation format was BPSK which offered 3 dB higher sensitivity and could be implemented using binary driving signals [69–71]. If BPSK is detected differentially, the need for a phase reference is eliminated and the complexity is still reasonable.

When the bandwidth supported by the EDFA (C-band $\sim$ 1530–1565 nm [41]) started to get filled, research on more spectrally efficient modulation formats gained more attention. By modulating the phase and/or the amplitude as well as utilizing both polarization states more signaling levels can be achieved and thus modulation formats that carry more bits per symbol can be used. Although modulation formats utilizing both the amplitude and the phase can be differentially detected [72] and polarization demultiplexing can be performed optically [73], coherent detection is preferred since the required subsystems that are complex in the optical domain, such as polarization and phase-tracking, can be moved to the DSP domain [53].

The most widely studied modulation format in coherent systems is PM-QPSK and there are many reasons for this. The transmitter complexity is low since it can be implemented with binary driving signals, the DSP algorithms, especially phase tracking, can be performed with reasonable complexity and the sensitivity of QPSK is suitable for long-haul distances such as transoceanic links. QPSK is also used in commercially deployed coherent fiber systems [74, 75]

PM-16QAM is often considered as the next step after PM-QPSK for transmission systems requiring a higher SE. The transmitter complexity is still reasonable, using 4-ary pulse amplitude modulation (4PAM) driving signals, yet more complex than PM-QPSK. The DSP algorithms are more complex, which is discussed in chapter 4. However, the sensitivity of PM-16QAM is worse compared to PM-QPSK which is a limiting factor in terms of transmission reach.

This chapter starts with the introduction of some basic concepts used to compare different modulation formats. Later, a few conventional modulation formats optimized in two dimensions are discussed followed by the introduction to four-dimensional (4D) modulation formats.

3.1 Basic Concepts and Notations

In this section modulation formats are studied assuming a discrete-time memoryless channel with AWGN as the only impairment. The kth symbol of a symbol alphabet is denoted as the vector

$$\mathbf{c}_k = (c_{k,1}, c_{k,2}, \ldots, c_{k,N}), \tag{3.1}$$

where N is the number of dimensions. The traditional view is to consider modulation formats in the two dimensions spanned by the in-phase and quadrature part of the signal such that the kth symbol can written as $\mathbf{c}_k = (\mathrm{Re}(E_{x,k}), \mathrm{Im}(E_{x,k}))$, where $E_{x,k}$ is the optical field. A 4D symbol, assuming that the four dimensions are the I- and Q-components of the two polarization states, can be denoted as $\mathbf{c}_k = (\mathrm{Re}(E_x), \mathrm{Im}(E_x), \mathrm{Re}(E_y), \mathrm{Im}(E_y))$ where E_x and E_y denotes the optical field in the x- and y-polarization state, respectively.

The symbol alphabet, or constellation, of a modulation format with M symbols is given by the set of vectors

$$\mathcal{C} = \{\mathbf{c}_1, \mathbf{c}_2, \ldots, \mathbf{c}_M\}. \tag{3.2}$$

With this notation, the QPSK constellation can be expressed as $\mathcal{C}_{\text{QPSK}} = \{(\pm 1, \pm 1)\}$ and PM-QPSK as $\mathcal{C}_{\text{PM-QPSK}} = \{(\pm 1, \pm 1, \pm 1, \pm 1)\}$.

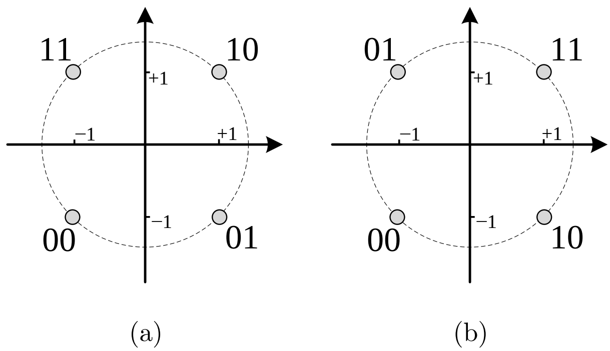

Figure 3.1: Examples of bit-to-symbol mapping with (a) the natural mapping and (b) Gray coded bit-to-symbol-mapping.

The average symbol energy E_s of a modulation format with M symbols is given by

$$E_s = \frac{1}{M}\sum_{k=1}^{M} ||\mathbf{c}_k||^2, \tag{3.3}$$

where $||\mathbf{c}_k||^2$ is the energy of the kth symbol. The average energy per bit is simply $E_b = E_s/\log_2(M)$.

The Euclidean distance between two symbols is given by $d_{k,j} = ||\mathbf{c}_k - \mathbf{c}_j||$. At high SNR, the sensitivity of a modulation format is determined by the average symbol energy and minimum Euclidean distance [76] of the constellation which is given by

$$d_{\min} = \min_{j\neq k} d_{k,j}. \tag{3.4}$$

3.1.1 Bit-to-Symbol Mapping

The performance in terms of bit-error probability (BER) at a certain SNR is dependent on how bits are mapped to symbols. The probability of making an error from one symbol to a symbol at distance $d_{\min}$ is higher than making an error to a symbol at $d > d_{\min}$. Therefore, a common aim of the bit-to-symbol mapping is to try to minimize the number of bits that will be erroneous when making an error between symbol pairs at the Euclidean distance $d_{\min}$ from each other. As an example, a QPSK constellation with a certain bit-to-symbol mapping is shown in Fig. 3.1a. As seen, if an error is made between $(-1,-1)$ and $(-1,1)$ both bits will be erroneous. In Fig. 3.1b, a different bit-to-symbol mapping is used such that all errors made to a symbol at $d_{\min}$ will result in exactly 1 bit error. This is usually referred to as *Gray coding* [77] and it should be noted that some constellations can be Gray coded in different ways where the optimal in terms of BER for all SNR values except extremely low, assuming quadrature amplitude modulation (QAM) or phase shift keying (PSK) constellations, is the *binary reflected Gray code* [78].

3.2 Spectral Efficiency and Asymptotic Power Efficiency

To compare the performance of different modulation formats at higher SNR, without performing time-consuming simulations, the SE and asymptotic power efficiency (APE) can be used. However, the performance depends on many other aspects such as sensitivity at low SNR, nonlinear performance and implementation complexity. In the following, AWGN will be considered as the only impairment.

3.2.1 Spectral Efficiency

When modulation formats are compared in terms of SE and APE, the SE is generally defined as the number of transmitted bits per polarization, i.e. per pair of dimensions, as

$$\mathrm{SE} = \frac{\log_2(M)}{N/2}, \tag{3.5}$$

where M is the number of symbols in the constellation and N the dimensionality [76]. In other words, $\log_2(M)$ is the number of bits per symbol and the unit of SE is *bits/symbol/polarization* (*bits/symb/pol*). It should be noted that this is a slightly different measure than bits/second per bandwidth use, $bits/s/Hz$, where information on the spectral shape is needed.

3.2.2 Asymptotic Power Efficiency

The APE is a good measure of how sensitive a modulation format is at asymptotically high SNR. The APE is given as [42, Section 5.1.2]

$$\gamma = \frac{d_{\min}^2}{4E_b} = \frac{d_{\min}^2 \log_2(M)}{4E_s}. \tag{3.6}$$

The factor 1/4 normalizes the APE to 0 dB for BPSK, QPSK and PM-QPSK [76]. The APE is often given in dB and it is also common to use the *asymptotic power penalty* which is defined as $1/\gamma$.

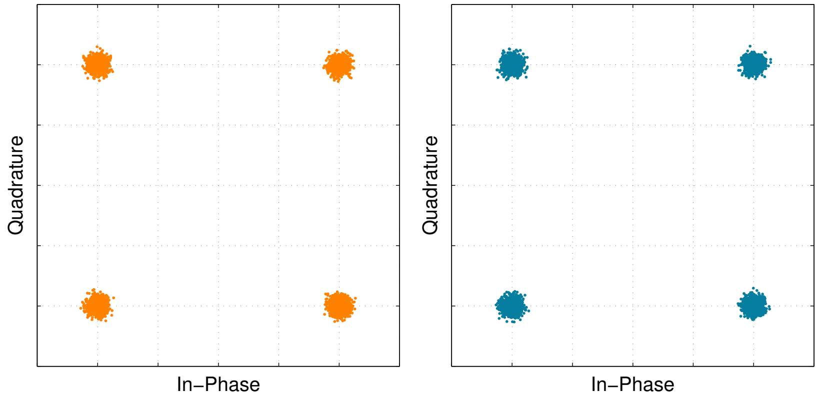

(a) x-polarization (b) y-polarization

Figure 3.2: Example of a PM-QPSK signal showing the constellation in the (a) x-polarization and (b) y-polarization.

3.3 Conventional Modulation Formats for Coherent Systems

In this section the most commonly studied modulation formats for coherent fiber optical communication systems are presented. Although OOK historically has been a much used format in direct-detection systems it is of little use in coherent systems where the access to the full optical field offers a possibility to use more spectrally efficient and/or more sensitive formats. The conventional modulation formats are given in the two dimensions spanned by the in-phase and quadrature components of the optical field and the polarization states are seen as two independent channels where these two-dimensional (2D) formats can be transmitted to double the throughput.

3.3.1 Polarization-Multiplexed Quadrature Phase Shift Keying

PM-QPSK is the most studied modulation format in coherent fiber optical communication systems [36]. As mentioned in the introduction to this chapter, there are many reasons for this such as good sensitivity and low complexity in terms of hardware and receiver DSP. The constellation for PM-QPSK is given by all sign selections of

$$\mathcal{C}_{\text{PM-QPSK}} = \{(\pm 1, \pm 1, \pm 1, \pm 1)\}. \tag{3.7}$$

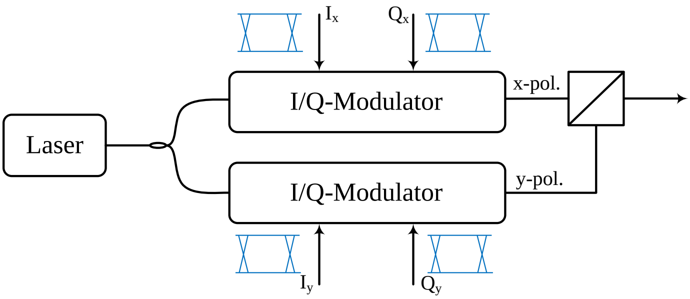

Figure 3.3: A typical PM-QPSK transmitter.

The constellation in the x- and y-polarization for PM-QPSK is shown in Fig. 3.2. Note that the constellations in the two polarization states are independent. PM-QPSK has $\gamma = 0$ dB and SE = 2 bits/symb/pol.

A typical transmitter for PM-QPSK is shown in Fig. 3.3. As seen the transmitter is based on two I/Q-modulators, one for each polarization. The I/Q-modulators are driven by binary drive signals which typically are optimized to have a voltage swing of $2V_\pi$. The two optical signals are combined with orthogonal polarization states using a polarization beam combiner (PBC). QPSK modulation can also be implemented using a phase modulator or a Mach-Zehnder modulator (MZM) followed by a phase modulator [79].

It is interesting to note that QPSK is inherently Gray-coded when implemented using an I/Q-modulator and binary driving signals. However, it is also common to use differential coding in the case where resilience towards cycle slips in the phase tracking (discussed in section 4.5.2) is needed.

3.3.2 Polarization-Multiplexed Binary Phase Shift Keying

BPSK has the same APE and SE as QPSK, since $N = 1$ in equation (3.5). However, if polarization-multiplexed BPSK (PM-BPSK) is considered and it is assumed that both quadratures are used, PM-BPSK will carry two bits per polarization-multiplexed symbol, compared to four of QPSK and the SE will be half compared to PM-QPSK. The transmitter as well as the receiver complexity for BPSK is roughly the same compared to QPSK and the DSP algorithms are very similar for the two formats. The constellation for PM-BPSK can be written

$$\mathcal{C}_{\text{PM-BPSK}} = \{(\pm 1, 0, \pm 1, 0)\}. \tag{3.8}$$

The constellations in the x- and y-polarization for PM-BPSK are shown in Fig. 3.4. Although QPSK is often preferred over BPSK for coherent systems

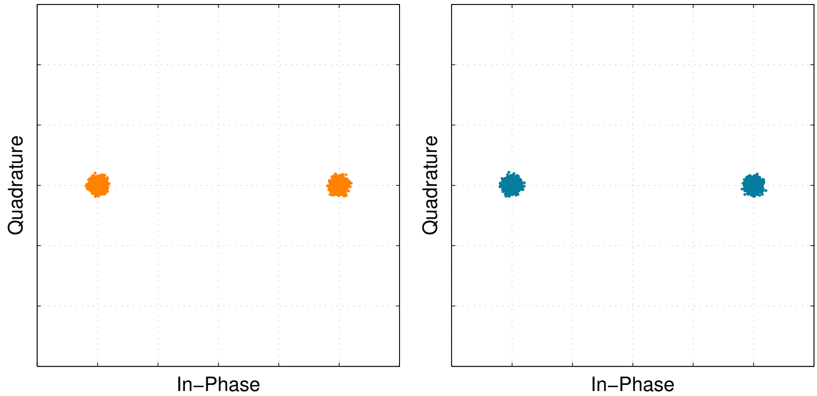

(a) x-polarization (b) y-polarization

Figure 3.4: Example of a PM-BPSK signal showing the constellation in the (a) x-polarization and (b) y-polarization.

some special applications exist such as *nonlinear squeezing* in highly non-linear fiber links with optimized dispersion maps where the nonlinear distortion can be made approximately imaginary whereas the BPSK modulation is real [80].

3.3.3 Polarization-Multiplexed 16-ary Quadrature Amplitude Modulation

In this thesis, and in general, 16-ary quadrature amplitude modulation (16QAM) refers to the square implementation of 16QAM although other implementations exist such as star-QAM [81], hexagonal 16QAM [82] and other 16-point ring constellations [83]. Rectangular 16QAM has the benefit that it can be implemented using equispaced 4-level signals which can be achieved in the electrical domain by combining two binary signals with an RF coupler. The constellation for PM-16QAM can be given as

$$\mathcal{C}_{\text{PM-16QAM}} = \{(\{\pm 1, \pm 3\}, \{\pm 1, \pm 3\}, \{\pm 1, \pm 3\}, \{\pm 1, \pm 3\})\}. \tag{3.9}$$

PM-16QAM has an APE of $\gamma = -3.97$ dB and a SE of 4 bits/symb/pol and the constellations in the x- and y-polarization are shown in Fig. 3.5. A typical PM-16QAM transmitter is shown in Fig. 3.6. As seen, the I/Q-modulators are driven by 4PAM signals generated from binary signals. This type of transmitter was implemented in paper A. Other transmitter structures exists, such as using two I/Q-modulators in series [84] or using integrated modulators with

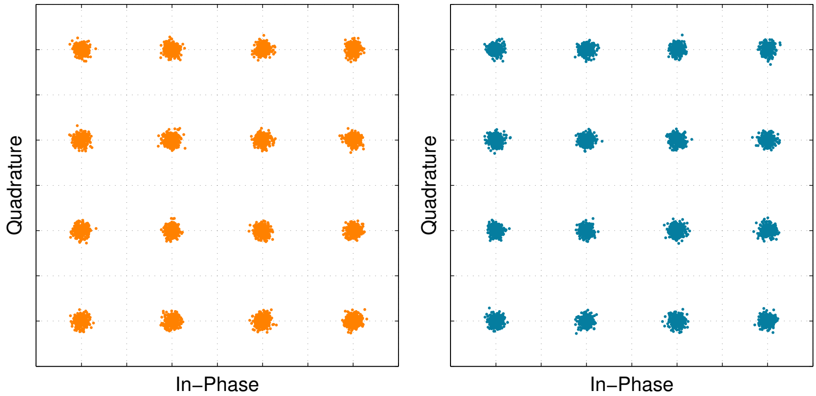

(a) x-polarization (b) y-polarization

Figure 3.5: Example of a PM-16QAM signal showing the constellation in the (a) x-polarization and (b) y-polarization.

four MZMs [85]. In contrast to QPSK, PM-16QAM is not inherently Gray-coded and a precoding stage is needed. Since PM-16QAM is more sensitive to laser phase noise, differential coding of the bits may be needed [86]. Alternatively, transmitting Gray-coded data in frames could possibly also handle this problem where a cycle slip would make the whole frame erroneous.

3.4 Four-Dimensional Modulation Formats

The conventional modulation formats, discussed in the previous sections, are optimized in the two dimensions spanned by the quadratures of the optical signal and the two orthogonal polarization states are used to multiplex the 2D formats. Instead modulation formats can be optimized in the 4D space spanned by the two quadratures and the two polarization states of the optical signal. These formats are often called 4D modulation formats and as the name implies the formats cannot be decomposed into two independent 2D constellations. The idea of 4D modulation formats for optical communication systems was first brought up during the 1990's when coherent communication was a hot research topic for a few years [87–89]. However, the complexity of implementing transmitters and receiver with the hardware available at that time as well as that fact that DSP was not used, prevented experimental realization of such formats.

In 2009 Bülow [90] as well as Agrell and Karlsson [76, 91] introduced modulation formats that are optimized in the 4D space to the fiber optical

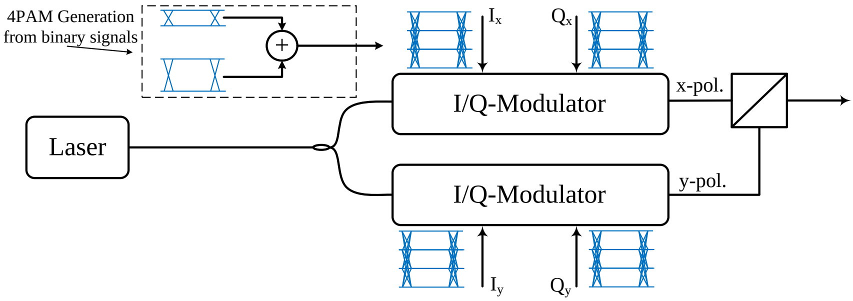

Figure 3.6: A typical PM-16QAM transmitter.

community. Bülow introduced Polarization-QAM (POLQAM), also known as 6-level polarization shift keyed QPSK (6polSK-QPSK), [90, 92] with six state-of-polarization (SOP) and four phase states per SOP has both better APE and SE compared to QPSK [76]. Agrell and Karlsson introduced PS-QPSK, which can be generated by transmitting QPSK in either the x- or y-polarization per 4D symbol. With this implementation, two bits are encoded in the QPSK constellation and one bit in which polarization this QPSK signal is transmitted. PS-QPSK was found to be the most power efficient modulation format in four dimensions [76].

Although PS-QPSK was a new format for the fiber optical communication community, the format itself was not new. In 1977 Zetterberg and Brändström mentioned this format where it is referred to as the 16-cell [93]. Many years later, the format was first studied in terms of APE [89]. In these publications the four dimensions are more general and from a communications theory point of view all realizations of the four dimensions are the same and are not restricted to the polarizations as the name PS-QPSK implies.

Another group of 4D modulation formats was introduced by Coelho and Hanik in 2011 [94]. These formats apply Ungerboeck's set-partitioning (SP) scheme [95] on PM-16QAM to increase the minimum Euclidean distance of the constellation. This concept was later extended to higher order rectangular QAM constellations [96]. When compared to the QAM constellations, the SP formats can achieve significant gains in APE while suffering only minor losses in SE. The two most notable SP formats are 128-SP-QAM, studied in paper A, and 32-level set-partitioning QAM (32-SP-QAM). As mentioned, these formats are based on QAM constellations which means that they can be implemented with similar hardware.

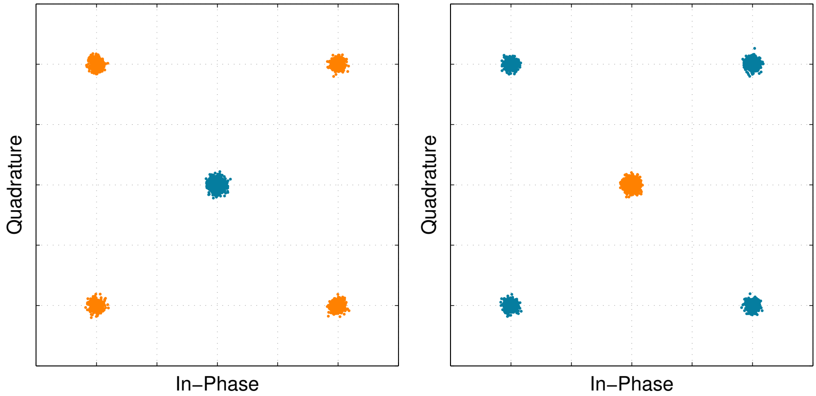

(a) x-polarization (b) y-polarization

Figure 3.7: Example of a PS-QPSK signal showing the constellation in the (a) x-polarization and (b) y-polarization. Orange and blue colors are used to illustrates that when a QPSK symbol is transmitted in one polarization, zero power is always transmitted in the other.

3.4.1 Polarization-Switched Quadrature Phase Shift Keying

PS-QPSK is the 4D modulation format, that cannot be constructed by polarization-multiplexing of two 2D formats, that has attracted the most research attention. The are many reasons for this, it can be implemented with only minor modifications to a conventional PM-QPSK transmitter and with binary driving signals. Further, the DSP architecture is similar to that of QPSK where the only difference is the adaptive equalizer which is discussed in section 4.4.1 [97].

The symbol alphabet for PS-QPSK can be given as

$$\mathcal{C}_{\text{PS-QPSK}} = \{(\pm 1, \pm 1, 0, 0), (0, 0, \pm 1, \pm 1)\}. \tag{3.10}$$

This constellation, shown as the IQ-planes in the x- and y-polarization, is illustrated in Fig. 3.7. PS-QPSK has γ =1.76 dB and SE = 1.5 bits/symb/pol. As seen from the constellations, PS-QPSK can be viewed as a QPSK symbol transmitted in either the x- or the y-polarization. Hence, 2 bits are encoded in the QPSK symbol and 1 bit in the polarization selection. The constellation $\mathcal{C}_{\text{PS-QPSK}}$ (3.10) will have $d_{\text{min}} = 2$ which is the same as for PM-QPSK but E_{s} is reduced to 2 which is half of that of PM-QPSK and this is why γ is increased to 1.76 dB.

Another way to derive PS-QPSK is to start with a PM-QPSK symbol alphabet and apply set-partitioning which yields two sub-sets with even and odd parity, respectively. The constellation for such a sub-set is given as

$$\mathcal{C}'_{\text{PS-QPSK}} = \pm\{(1,1,1,1),(1,1,-1-1),(1,-1,1,-1),(1,-1,-1,1)\}, \quad (3.11)$$

and has $d_{\min} = 2\sqrt{2}$ and the same $E_{\rm s}$ as PM-QPSK, which also yields $\gamma =$ 1.76 dB. In fact, it is possible to move between these two views of the PS-QPSK constellations by performing a rescaling and a 45° polarization rotation [91].

These two views have resulted in different transmitter implementations of PS-QPSK. The first type of transmitter, based on the polarization-switching view of PS-QPSK given in (3.10), is shown in Fig. 3.8a where an in-phase and quadrature-modulator (I/Q-modulator) is used to modulate a QPSK signal. This signal is then split into two arms with one MZM in each, driven in a push-pull configuration from a binary pattern so that the signal is switched between the two arms. The signal is then combined using a PBC with orthogonal polarizations. This type of transmitter was used in the first experimental demonstration of PS-QPSK [98] as well as in numerous other investigations [99–101].

A second type of transmitter is shown in Fig. 3.8b and is based on the set-partitioning view of PS-QPSK given in (3.11). This type utilizes the fact that if the fourth driving signal is formed by an exclusive or (XOR) operation on the three other binary driving signals, only the even parity sub-set of PM-QPSK is obtained. This type of transmitter has been experimentally implemented in [102, 103]. This is also the transmitter type that was used in paper B. Compared to the polarization-switching based transmitter this type of transmitter generally has lower implementation penalty due to the fact that the MZMs typically have limited extinction ratio and higher loss compared to two parallel I/Q-modulators. However, for a commercial system, XOR-gates with sufficiently high bandwidth has to be used which adds to the complexity while in an experimental demonstration the XOR-operation can be achieved by programming of one pattern.

A third type of transmitter which is very similar to the MZM based transmitter were demonstrated in [104] where a polarization-modulator [105] is used instead of the polarization-switching based on MZMs. Further, integrated PS-QPSK transmitters have been fabricated where extra coupling loss compared to an I/Q-modulator can be avoided [106].

PS-QPSK has been shown to achieve significant increase in transmission reach compared to PM-QPSK. In [99], 30 % increase in transmission is reported when the two formats are compared in a WDM system at the same bit rate of 42.9 Gbit/s. In paper B, 50 % increase is achieved when comparing the two formats at the same symbol rate and in a dual-carrier setup.

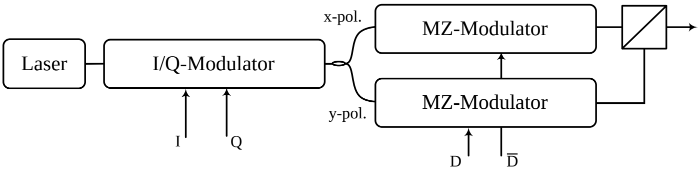

(a) Polarization-switching implementation.

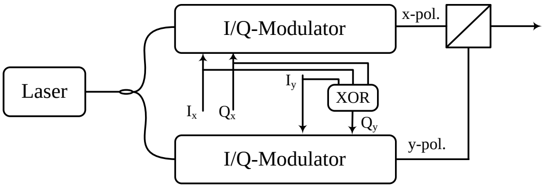

(b) Set-partitioning implementation.

Figure 3.8: Two possible experimental realizations of PS-QPSK showing (a) a transmitter based on polarization-switching using one MZM in each of the two polarizations. The MZMs are driven in a push-pull configuration so that the QPSK signal generated by the I/Q-modulator is only present in one of the polarization states at the time. (b) A transmitter based on set-partitioning where the Q_y is formed by an XOR-operation on the other three binary driving signals.

PS-QPSK has also been proposed as a backup solution for degrading channels where the idea is to have a flexible transmitter and receiver structure that can switch between PM-QPSK and PS-QPSK [107]. A similar idea was discussed in [108], where a flexible system is proposed that again can switch between PM-QPSK and PS-QPSK depending on the transmission reach that is desired. In both these publications the symbol rate is kept constant. A flexible coherent receiver architecture, enabled by data-aided training sequences, capable of switching between PM-QPSK and PS-QPSK was demonstrated with experimental data in [109, 110].

3.4.2 Binary Pulse Position Modulation Quadrature Phase Shift Keying

pulse position modulation (PPM) encodes data by transmitting a pulse in one of K consecutive slots, as illustrated with $K = 2$ in Fig. 3.9. The pulses can also be modulated with a 2D format such as QPSK which will be denoted

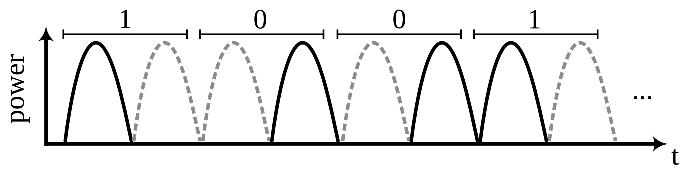

Figure 3.9: Example of a 2PPM pattern. As seen, a “1” is encoded as “10” and a “0” as “01”. Solid lines denote that a pulse was transmitted and dashed line that no pulse was transmitted.

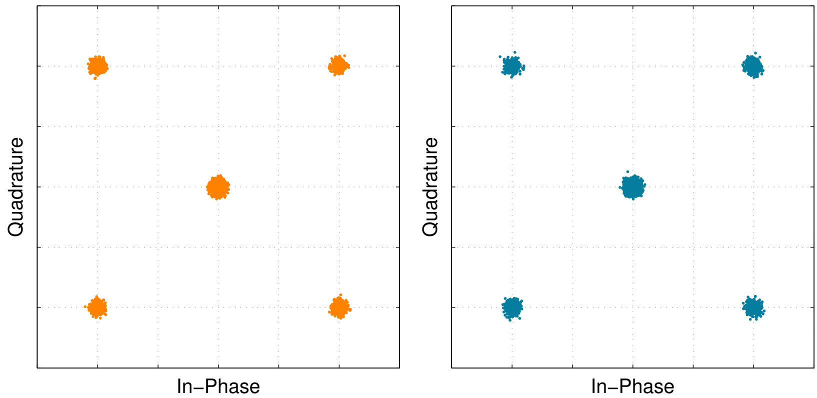

(a) x-polarization (b) y-polarization

Figure 3.10: Example of a PM-2PPM-QPSK signal showing the constellation in the (a) x-polarization and (b) y-polarization.

as binary pulse position modulation QPSK (2PPM-QPSK). Geometrically, 2PPM-QPSK is the same modulation format as PS-QPSK which can be understood from (3.10) where the four dimensions can be realized by the two quadratures of two consecutive time slots instead of two polarization states. The symbol alphabet of 2PPM-QPSK is given by

$$\mathcal{C}_{\text{2PPM-QPSK}} = \{(\pm1, \pm1, 0, 0), (0, 0, \pm1, \pm1)\}, \tag{3.12}$$

which is identical to (3.10). This means of course that 2PPM-QPSK has the same APE and SE as PS-QPSK. The constellation for 2PPM-QPSK is shown in Fig. 3.10. It should be noted that when utilizing the two polarization states with 2PPM-QPSK, it is easy to confuse the two possible implementations that exists, namely PM-2PPM-QPSK and 2PPM-PM-QPSK. With

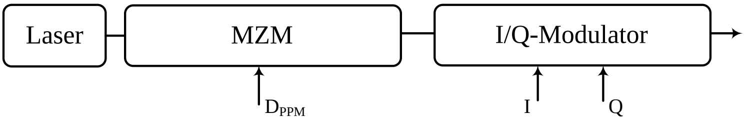

Figure 3.11: A typical 2PPM-QPSK transmitter. D_{PPM} denotes a 2PPM pattern, as illustrated in Fig. 3.9, that is generated from a binary sequence such that for instance a "1" generates the sequence "10" and a "0" generates "01".

PM-2PPM-QPSK, 2PPM-QPSK is transmitted independently in the two polarizations whereas for 2PPM-PM-QPSK the PPM is performed over time slots containing both polarizations. 2PPM-PM-QPSK has $\gamma = 0.97$ and SE = 1.25 bit/symb/pol which worse both in terms of APE and SE compared to PM-2PPM-QPSK.

A typical transmitter for 2PPM-QPSK is shown in Fig. 3.11. The MZM is driven by a binary PPM-pattern such that a "1" is encoded as "10" and a "0" as "01". The MZM is followed by an I/Q-modulator to modulate QPSK on the PPM pulses. The I/Q-modulator can be driven at half the repetition rate compared to the MZM since the QPSK symbol is extended over two time slots. The same transmitter can then be used in two orthogonal polarization states for polarization-multiplexing or for experimental investigations a polarization-multiplexing emulation stage based on split and time delay can be used. This is the type of transmitter that was used in paper C where the first experimental realization of 2PPM-QPSK was presented. In this paper, it is shown that 2PPM-QPSK can achieve 40 % increased transmission reach compared to PM-QPSK in a single channel system.

3.4.3 Set-partitioning QAM

PM-16QAM is often regarded as the next step after PM-QPSK when higher SE is desired. However, PM-16QAM has 3.97 dB worse power efficiency compared to PM-QPSK, which translates into a much shorter transmission distance. In the quest to find spectrally efficient modulation formats with better APE than PM-16QAM without too high complexity, Coelho and Hanik introduced a family of modulation formats than apply Ungerboeck's set-partitioning scheme [95] on PM-16QAM [94]. The formats proposed in [94] are 128-SP-QAM and 32-SP-QAM which will both be discussed in the following.

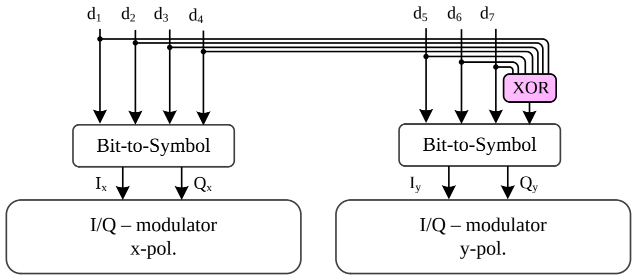

Figure 3.12: Generating 128-SP-QAM using an XOR-operation.

128-SP-QAM

128-SP-QAM can be derived from the Gray-coded PM-16QAM symbol alphabet where the even or the odd subset, obtained by an SP-operation, is chosen. This can be realized by forming one bit stream by an XOR-operation on the other 7 bit streams, as illustrated in Fig. 3.12. The transmitter is otherwise identical to that of PM-16QAM shown in Fig. 3.6. With this operation, only 128 of the 256 symbols from the PM-16QAM alphabet are allowed thus reducing the number of bits per symbol to 7 from 8. However, the minimum Euclidean distance is increased by a factor of $\sqrt{2}$ compared to PM-16QAM which gives 128-SP-QAM an APE of $\gamma = -1.55$ dB which is an increase of 2.43 dB over PM-16QAM. However, this comes at the cost of a reduced SE from 4 bit/symb/pol to 3.5 bit/symb/pol.

128-SP-QAM was first studied with numerical simulations in [111] where the format was compared to PM-QPSK and 8-ary quadrature amplitude modulation (8-QAM) where parts of the extra overhead available by going to a more spectral efficient format was used for soft-decision low-density parity check (LDPC) codes [112]. A more extensive numerical study was done in [113] where 128-SP-QAM was compared to PM-16QAM in a WDM scenario. Both these two studies identify 128-SP-QAM as an interesting format for spectrally efficient systems.

The first experimental demonstrations of 128-SP-QAM were done for a single channel in [114] and for WDM in [115]. In paper A an extension of the work in [114] was presented. It was shown that 128-SP-QAM can achieve 54 % longer transmission reach compared to PM-16QAM in a WDM system compared at the same aggregate bit rate. A record SE-distance product was set in [116], where time-interleaving of PM-16QAM and 128-SP-QAM together with forward error correction (FEC) based on LDPC with long codeword and large overhead were key-points in achieving the record.

Other SP-formats

32-SP-QAM is also derived from PM-16QAM but keeping only 32 symbols with increased minimum Euclidean distance compared to 128-SP-QAM. 32-SP-QAM has the same APE of $\gamma = 0$ dB as PM-QPSK but with an increased SE to 2.5 bit/symb/pol which is an increase of 0.5 bit/symb/pol over PM-QPSK [96]. In the numerical studies in [111], the sensitivity of 32-SP-QAM is shown to be similar to that of PM-QPSK when compared with LDPC coding. In the numerical simulations in [117], 32-SP-QAM was compared to a system interleaving QPSK and 8-QAM which yields the same SE for both systems and 32-SP-QAM was found to perform slightly better in terms of back-to-back (B2B) sensitivity and nonlinear transmission. 32-SP-QAM was experimentally demonstrated in [115] where the transmission reach was roughly 50 % shorter than PM-QPSK.

512-ary set-partitioning QAM (512-SP-QAM) is generated by set-partitioning on the polarization-multiplexed 64-ary quadrature amplitude modulation (PM-64QAM) symbol alphabet, in the same way as 32-SP-QAM is generated from PM-16QAM. 512-SP-QAM has $\gamma = -3.68$ dB and SE $= 4.5$ bit/symb/pol [96]. Even though the complexity of generating this format is high, it has the interesting feature of having both higher APE and SE than PM-16QAM.

3.4.4 Other 4-dimensional modulation formats

$\mathcal{C}_{\mathrm{opt},16}$ is a 16-point 4D format that was found by sphere packing and has 1.11 dB increased power efficiency over PM-QPSK with a maintained SE of 2 bit/symb/pol [118]. This is the best 16-point 4D modulation format that is known. $\mathcal{C}_{\mathrm{opt},16}$ has been experimentally investigated in a B2B scenario of an orthogonal frequency division multiplexing (OFDM) system where a gain at low OSNR over PM-QPSK in terms of the symbol error probability (SER) was seen and it was concluded that with optimal coding $\mathcal{C}_{\mathrm{opt},16}$ can achieve higher SE [119]. $\mathcal{C}_{\mathrm{opt},16}$ has also been experimentally investigated over a 480 km link where data-aided training sequences were used to enable polarization demultiplexing and equalization [120].

Modulating the state of polarization to carry data was investigated theoretically in [121]. However, in this study the absolute phase of the signals was not considered which prevents many possible formats. 6polSK-QPSK, first introduced by Bülow [90], utilizes 6 SOPs with 4 phase states each. 6polSK-QPSK has SE $= 2.25$ bit/symb/pol and $\gamma = 0.51$ dB which reveals that it is both more power efficient and spectrally efficient than QPSK. The first experimental realization of 6polSK-QPSK was done in [122, 123] where both experiments were done at a symbol rate of 28 Gbaud and where in [122] the format was demonstrated B2B with blind equalization and phase tracking. In

[123], 6polSK-QPSK was demonstrated in transmission and data-aided pilot sequences were used for equalization and phase estimation.

Subset-optimized PM-QPSK (SO-PM-QPSK) optimizes the amplitude ration between the even and odd subset, obtained by set-partitioning of PM-QPSK, to increase the power efficiency. With the optimal amplitude ratio, SO-PM-QPSK has 0.44 dB increased APE over QPSK [124].

3.5 8-dimensional Modulation Formats

Given the plethora of novel modulation formats with interesting features that was enabled by considering modulation in the 4D of the optical field rather than polarization-multiplexing of 2D modulation formats, it is only natural to consider increasing the dimensionality to 8. However, since the optical field only has 4-dimensions, some way to increase the dimensionality has to be used to achieve an eight-dimensional (8D) signal space. For instance, two different wavelength channels can be used to achieve the 8 dimensions as was done in paper B. Alternatively, two consecutive time slots can be used as in [125]. Other possibilities include using different modes to increase the dimensionality [126] or different cores of a multicore fiber.

In paper B biorthogonal modulation in 8 dimensions was proposed and experimentally investigated for coherent fiber optical systems. Biorthogonal modulation can be described as transmitting energy in only one dimension at the time, and the amplitude in each dimension can only be $\pm a$ where a is the amplitude and for the rest of this section $a = 1$ will be used for simplicity [43, p. 111]. To study 8D biorthogonal modulation is a natural step, which can be understood from table 3.1 which shows biorthogonal modulation in N dimensions, where $N = 1$, 2, 4 and 8 together with the name of the corresponding modulation format. As seen, in one dimension biorthogonal modulation corresponds to BPSK and in two dimensions to QPSK. In four dimensions, it corresponds to PS-QPSK which, as discussed in the previous sections, has been extensively studied for coherent optical systems in recent years. Geometrically, biorthogonal modulation is the N-dimensional cross-polytope for which an exact SER expression were given in [127].

The constellation for 8D biorthogonal modulation is given as

$$\begin{aligned}\mathcal{C}_{\text{8D-biorthognoal}} =&\{(\pm1,0,0,0,0,0,0,0),(0,\pm1,0,0,0,0,0,0),\\&(0,0,\pm1,0,0,0,0,0),(0,0,0,\pm1,0,0,0,0),\\&(0,0,0,0,\pm1,0,0,0),(0,0,0,0,0,\pm1,0,0),\\&(0,0,0,0,0,0,\pm1,0),(0,0,0,0,0,0,0\pm1)\}.\end{aligned} \tag{3.13}$$

8D biorthogonal modulation has $\gamma = 3$ dB and SE = 1 bit/symb/pol. This format can be generated in different ways, for instance two time slots can be

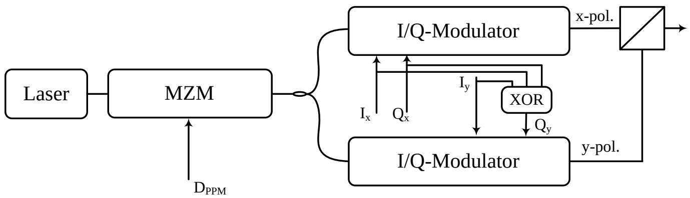

(a) time-domain implementation.

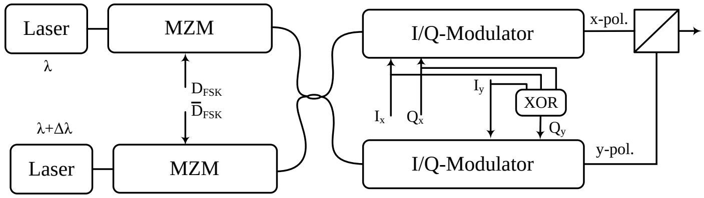

(b) frequency-domain implementation.

Figure 3.13: Transmitter structures for two different implementations of 8D biorthogonal modulation showing (a) a transmitter based on 2PPM where the MZM is driven by a 2PPM-pattern and the two I/Q-modulators are driven to generate PS-QPSK. (b) A transmitter based on FSK where the two MZMs are driven in a push-pull configuration so that only one laser is active at the time. The I/Q-modulators are again modulating PS-QPSK.

considered which would yield a format that can be described as combining binary pulse position modulation (2PPM) with PS-QPSK. A possible transmitter for this realization is shown in Fig. 3.13a, where 2PPM modulation is followed by a PS-QPSK transmitter based on the set-partitioning principle described in section 3.4.1. With this view, 1 bit is encoded in the 2PPM and 3 bits in the PS-QPSK modulation. In paper B another realization is done, two wavelength channels were used to realize the 8 dimensions instead of two time-slots. The transmitter structure that was used is shown in Fig. 3.13b and as seen two lasers with a wavelength separation $\Delta\lambda$ are used. After each laser a MZM is used and the two MZMs are driven in a push-pull configuration so that for each time-slot only one laser can be active at the time which acts as binary frequency shift keying (FSK). The frequency modulation stage is followed by a PS-QPSK transmitter. Hence, 1 bit is encoded in the FSK and 3 bits in the PS-QPSK modulation.

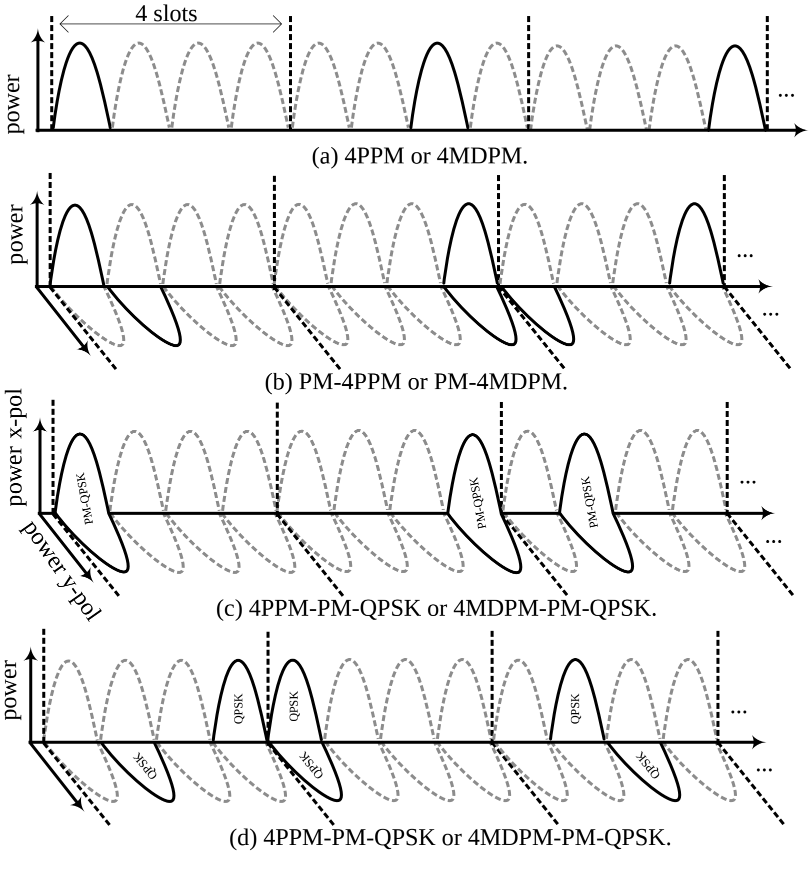

Figure 3.14: Different combinations of PPM (or seen as MDPM depending on what unit that is considered on the x-axis) showing (a) conventional 4PPM, (b) polarization-multiplexed 4PPM (PM-4PPM), (c) 4PPM in combination with PM-QPSK (4PPM-PM-QPSK), (d) polarization-multiplexed 4PPM-QPSK (PM-4PPM-QPSK).

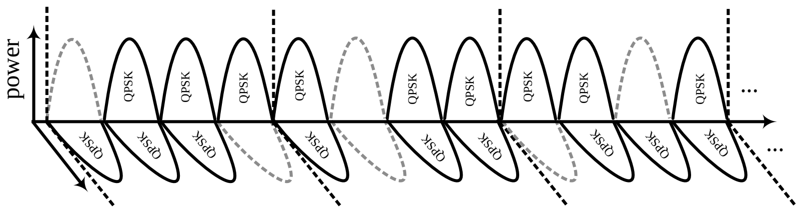

(a) PM-4iPPM-QPSK or PM-4iMDPM-QPSK.

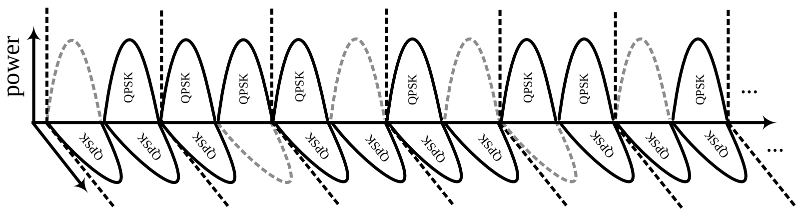

(b) 4iPPM-QPSK or 4iMDPM-QPSK.

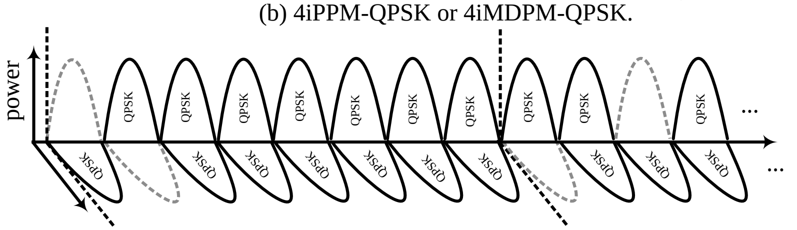

(c) PM-8iPPM-QPSK or PM-8iMDPM-QPSK.

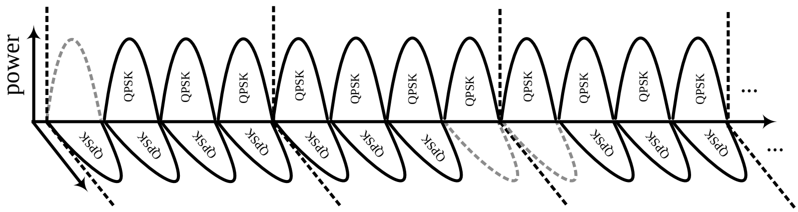

(d) 8iPPM-QPSK or 8iMDPM-QPSK.

Figure 3.15: Different implementations of KiMDPM-QPSK showing (a) an implementation of 4iMDPM-QPSK using 4 slots in one polarization and then polarization-multiplexing of the signal (PM-4iMDPM-QPSK), (b) another possible implementation of 4iMDPM-QPSK utilizing 2 slots in each polarization, (c) an implementation of 8iMDPM-QPSK using 8 slots in one polarization and then polarization-multiplexing of the signal (PM-8iMDPM-QPSK), (d) another possible implementation of 8iMDPM-QPSK utilizing 4 slots in each polarization.

3.6 Multidimensional Modulation Formats

In 2011, Liu *et al.* were able to show a coherent optical transmission system with record high sensitivity of 3.5 photons per bit [128]. This was done by using 16-ary PPM (16PPM) in combination with PM-QPSK (16PPM-PM-QPSK). The high sensitivity could be achieved due to the fact that the dimensionality of the signal was increased by considering several time-slots as one symbol. This concept was later generalized in [129], where K-ary PPM (KPPM) in combination with QPSK, PM-QPSK and PS-QPSK is studied in terms of SE and APE. It was shown in [129] that the results in [128] could be improved if polarization-multiplexing of 16PPM-QPSK is considered instead since this format has both higher SE and APE than 16PPM-PM-QPSK [129].

For conventional PPM, only one pulse is transmitted per PPM-frame as illustrated in Fig. 3.14(a) and for a polarization-multiplexed PPM signal in Fig. 3.14(b). For coherent systems the pulse can also be modulated with an I/Q-modulation format, such as QPSK, as shown in Fig. 3.14(c) where the PPM is considered over both polarizations or as in Fig. 3.14(d) where instead the PPM is only considered over one polarization and the 4PPM-QPSK signal is polarization-multiplexed (giving PM-4PPM-QPSK). PPM is an effective and hardware-wise low-complex way of increasing the APE. However, the SE is reduced drastically for high order PPM.

Instead of using only one pulse per PPM frame, data can be encoded into transmitting several pulses per frame. This has been studied quite extensively for intensity modulated systems, where the concept is often denoted as multi-pulse position modulation (MPPM) [130, 131].

Table 3.1: Biorthogonal modulation in N-dimensions and the corresponding well-known modulation format

N (dimensions)	Modulation Format	SE†	APE	$M^\ddagger$
1	BPSK	2	0 dB	2
2	QPSK	2	0 dB	4
4	PS-QPSK	1.5	1.76 dB	8
8	4FPS-QPSK, paper B	1	3 dB	16

† in bit/symbol/polarization.
‡ number of symbols.

For coherent systems, not much research has been done on MPPM. The few exceptions include [132], where PPM in combination with PS-QPSK is studied and it was found that it is possible to achieve both higher SE and APE compared to PS-QPSK without any MPPM. Another exception is [133], where MPPM in combination with BPSK is studied for both coherent and direct detection systems. As mentioned for the 8D formats in section 3.5, other physical properties that time slots can be used to effectively increase the dimensionality of the signal space. In for instance [134], a combination of different frequencies, time-slots and polarization states are used. In paper D, MPPM in combination with QPSK, PM-QPSK and PS-QPSK is generalized for coherent communication systems. Instead of only considering time-slots, multidimensional position modulation (MDPM) is introduced where the different dimensions can be realized by using time-slots, polarizations, WDM-channels, modes of a multimode fiber or cores of a multicore fiber.

In paper D, a particularly interesting family of modulation formats was found which is denoted inverse-MDPM (iMDPM) due to the fact that these formats transmit exactly one slot with zero power per frame. This can be seen as the inverse of conventional position modulation where only one nonzero pulse is transmitted per frame. For these formats, KiMDPM in combination with I/Q-modulation will carry an integer number of bits per frame when K is a power of two. Two such formats are 4iMDPM-QPSK and 8iMDPM-QPSK. 4iMDPM-QPSK can for instance be implemented using PPM as illustrated in Fig. 3.15(a) where 4 time-slots are used and the signal is then polarization-multiplexed, or as in Fig. 3.15(b) where the 4 slots are obtained using 2 slots in each polarization. The same concept for 8iMDPM-QPSK gives the two possible implementations that are illustrated in Fig. 3.15(c) and Fig. 3.15(d).

The constellation for 4iMDPM-QPSK has $M = 256$ points that are given as

$$\begin{aligned}\mathcal{C}_{\text{4iMDPM-QPSK}} = \quad & \{(\pm1,\pm1,\pm1,\pm1,\pm1,\pm1,0,0),\\ & (\pm1,\pm1,\pm1,\pm1,0,0,\pm1,\pm1),\\ & (\pm1,\pm1,0,0,\pm1,\pm1,\pm1,\pm1),\\ & (0,0,\pm1,\pm1,\pm1,\pm1,\pm1,\pm1)\}.\end{aligned} \tag{3.14}$$

4iMDPM-QPSK is an 8D-format that has SE = 2 bit/symb/pol and an APE of $\gamma = 1.25$ dB. In other words, 4iMDPM-QPSK has the same SE as QPSK with an increased APE of 1.25 dB.

The constellation for 8iMDPM-QPSK has $M = 2^{17}$ symbols that are given as

$$\begin{aligned}
&\mathcal{C}_{\text{8iMDPM-QPSK}} = \\
&\{(\pm1,\pm1,\pm1,\pm1,\pm1,\pm1,\pm1,\pm1,\pm1,\pm1,\pm1,\pm1,\pm1,\pm1,0,0),\\
&(\pm1,\pm1,\pm1,\pm1,\pm1,\pm1,\pm1,\pm1,\pm1,\pm1,\pm1,\pm1,0,0,\pm1,\pm1),\\
&(\pm1,\pm1,\pm1,\pm1,\pm1,\pm1,\pm1,\pm1,\pm1,\pm1,0,0,\pm1,\pm1,\pm1,\pm1),\\
&(\pm1,\pm1,\pm1,\pm1,\pm1,\pm1,\pm1,\pm1,0,0,\pm1,\pm1,\pm1,\pm1,\pm1,\pm1),\\
&(\pm1,\pm1,\pm1,\pm1,\pm1,\pm1,0,0,\pm1,\pm1,\pm1,\pm1,\pm1,\pm1,\pm1,\pm1),\\
&(\pm1,\pm1,\pm1,\pm1,0,0,\pm1,\pm1,\pm1,\pm1,\pm1,\pm1,\pm1,\pm1,\pm1,\pm1),\\
&(\pm1,\pm1,0,0,\pm1,\pm1,\pm1,\pm1,\pm1,\pm1,\pm1,\pm1,\pm1,\pm1,\pm1,\pm1),\\
&(0,0,\pm1,\pm1,\pm1,\pm1,\pm1,\pm1,\pm1,\pm1,\pm1,\pm1,\pm1,\pm1,\pm1,\pm1)\}.
\end{aligned} \tag{3.15}$$

The dimensionality of 8iMDPM-QPSK is 16 and this format that has SE = 2.13 bit/symb/pol and an APE of $\gamma = 0.84$ dB. Thus, 8iMDPM-QPSK has slightly higher SE compared to QPSK with an increased APE of 0.84 dB.

Some examples of modulation formats and their representations using the MDPM notation introduced in paper D are shown in table 3.2 together with the dimensionality of the formats. Included in table 3.2 are also some references to either theoretical or experimental papers concerning the specific format.

3.7 Coding Representation of Modulation Formats

Applying FEC can be seen as increasing the dimensionality of the signal space. When higher dimensional modulation formats are considered it is therefore a vague line between what is a modulation format and what is an FEC code. For instance, PS-QPSK can be interpreted as a single parity check code on PM-QPSK [135, section 3.7]. The same holds for 128-SP-QAM which is a single parity check code on PM-16QAM. The PPM formats and the MDPM formats can be described as block codes [135, chapter 3] on the case of transmitting a certain modulation format or zero power in each slot.

3.8 Summary of the Experimentally Investigated Modulation Formats in this Thesis

The modulation formats that have been experimentally investigated in papers A–C are included in Fig. 3.16 where the bit rate per channel is plotted as a function of the obtained transmission reach at BER $= 10^{-3}$ and for the optimized launch power at this BER for all formats. However, it should be noted that a comparison like this has many uncertain factors. For example,

Table 3.2: Examples of modulation formats, their dimensionality and references to experimental or theoretical papers concerning the specific format

Modulation Format	$N^\dagger$	MDPM representation	Reference
QPSK	2	1MDPM-QPSK	
2PPM	2	2MDPM	[136]
PS-QPSK	4	2MDPM-QPSK	[91]
2PPM-QPSK	4	2MDPM-QPSK	C
4FPS-QPSK	8	4MDPM-QPSK	B
PolSK-4FSK	8	8MDPM	[134]
4iMDPM-QPSK	8	4iMDPM-QPSK	D
8iMDPM-QPSK	16	8iMDPM-QPSK	D
4PPM-PM-QPSK	16	4MDPM-PM-QPSK	[134]
8PPM-PS-QPSK	32	8MDPM-PS-QPSK	[129]
16PPM-PM-QPSK	64	16MDPM-PM-QPSK	[128]
64PPM-PS-QPSK	256	64MDPM-PS-QPSK	[137]
256PPM	256	256MDPM	[136]

† Number of dimensions

different symbol rates are used, some formats are implemented in a WDM setup and PM-QPSK as well as PS-QPSK in paper B are implemented in a dual-carrier setup where both channels are detected using the same hybrid. It should also be noted that the nonlinear distortions will behave differently for different symbol rates and number of WDM channels.

Another comparison is to plot the transmission reach at BER $= 10^{-3}$ for the formats in papers A-C as a function of the maximum SE, equation (3.5), which is shown in Fig. 3.17. This comparison assumes that a whole WDM system can be implemented with similar transmission reach as to the reported results, however it should be noted that comparing the single channel results with the WDM results for PM-16QAM and 128-SP-QAM it can be seen that the reduction in reach for going to WDM from single channel is in the range of 25–30 %. One qualitative conclusion from Fig. 3.17 is that the formats in papers A-C give a finer granularity when choosing modulation format depending on which transmission reach that is required. As seen, using a modulation format with extended reach comes at the expense of a reduced SE.

128-SP-QAM offers roughly 50 % longer transmission reach compared to PM-16QAM at the expense of a reduced SE by 0.5 bit/symb/pol. To extend the reach over PM-QPSK, PS-QPSK or 2PPM-QPSK can be used with 0.5

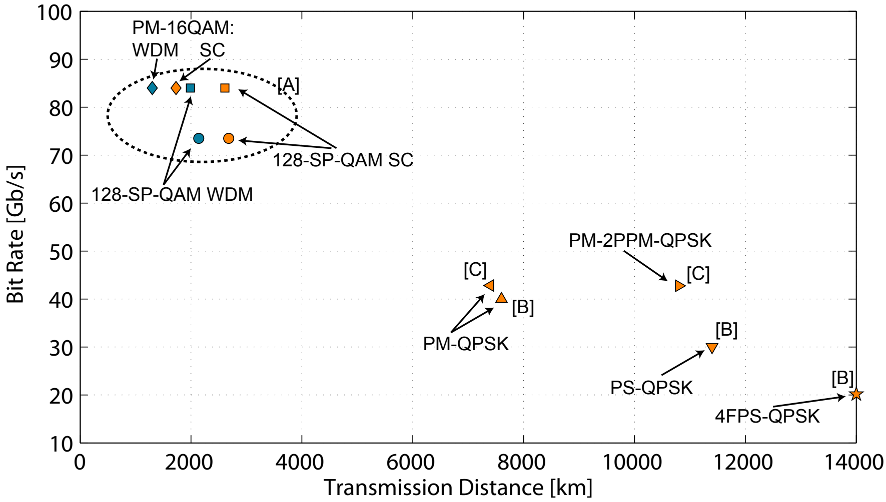

Figure 3.16: Bit rate per channel as a function of transmission reach at BER $= 10^{-3}$ for all formats experimentally investigated in paper A (dashed region), paper B and paper C. SC denotes single channel.

bit/symb/pol lower SE or if even longer transmission reach is required, 4FPS-QPSK can be used at the loss in SE of 1 bit/symb/pol. In between 128-SP-QAM and PM-QPSK there is a gap in terms of achievable transmission reach where not so much research has been done for 4D formats. For that reason it would be interesting to, in future work, investigate 32-SP-QAM and other formats around SE = 2.5–3 bit/symb/pol.

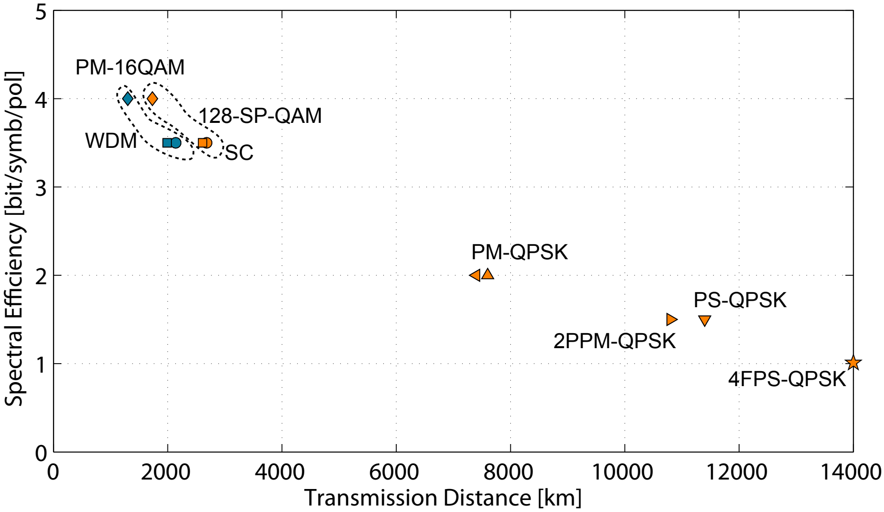

Figure 3.17: Maximum SE as a function of transmission reach at BER $= 10^{-3}$ for all formats experimentally investigated in papers A-C. SC denotes single channel.

Chapter 4

Digital Signal Processing

Much of the progress of coherent systems can be attributed to the use of DSP which, as mentioned in the introduction to chapter 3, allowed the use of free-running LOs where the phase-tracking is done in the digital domain rather than with complicated phase-locked loop schemes implemented in hardware. Further, the access to both the amplitude and the phase of the optical field allowed the use of spectrally efficient modulation formats as well as the possibility to mitigate different transmission impairments in the DSP. In this chapter, modulation format independent signal processing will be explained first followed by the description of methods that are used for different modulation formats. For all modulation formats discussed in this thesis, the DSP follows the blocks in Fig. 4.1. The different blocks have to be implemented with different algorithms depending on format and in some cases some blocks have to be implemented jointly with iterations between the blocks.

4.1 Optical Front-End Correction

The optical signal can be distorted by imperfections in the transmitter and and the receiver. In the transmitter, impairments such as non-ideal bias for the I and Q signals as well as the 90°-phase shift in the IQ-modulator, imperfect splitting ratio of the optical signal, different amplitude of the RF driving signals or different gain of the drive-amplifiers as well as non-ideal polarization splitting can distort the signal. The impairments in the receiver are mainly 90° hybrid imperfections and differing responsivities of the photo-detectors [138].

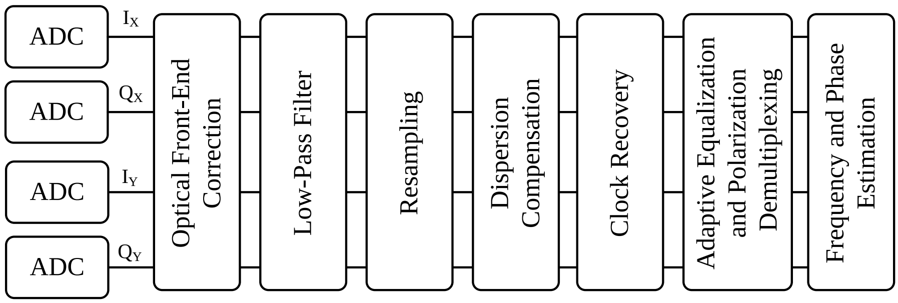

Figure 4.1: The typical digital signal processing blocks of a coherent receiver.

4.1.1 90° Hybrid Error

The in-phase and quadrature parts of the optical signal are ideally orthogonal. However, an imperfect 90° hybrid can cause the received signal to loose orthogonality. The detected signals in one polarization from the optical hybrid that has been sampled by the ADCs can be modeled as

$$r_{Ix} = \mathrm{Re}\left(i_x\right), \tag{4.1}$$

$$r_{Qx} = \mathrm{Re}\left(-ji_x \exp j\theta\right), \tag{4.2}$$

where i_x is the received complex signal and θ is the error in the 90° phase-shift in the optical hybrid. In the ideal case $\theta = 0$ and for any other θ the I and Q channels become non-orthogonal. Fig. 4.2a shows a QPSK constellation which was ideal in the transmitter and the only impairments are a remaining intermediate frequency (IF) and a 90° hybrid error of $\theta = 25°$.

4.1.2 Orthogonalization Algorithms

The most common orthogonalization algorithm is the Gram-Schmidt orthogonalization which can mitigate the distortions from imperfections in the 90° optical hybrid. The sampled signals r_I and r_Q can be transformed into a new pair of orthogonal signals using the following

$$I_{\mathrm{orthogonal}}(t) = \frac{r_I(t)}{\sqrt{P_I}}, \tag{4.3}$$

$$Q'(t) = r_Q(t) - \frac{\langle r_I(t) \cdot r_Q(t)\rangle\, r_I(t)}{P_I}, \tag{4.4}$$

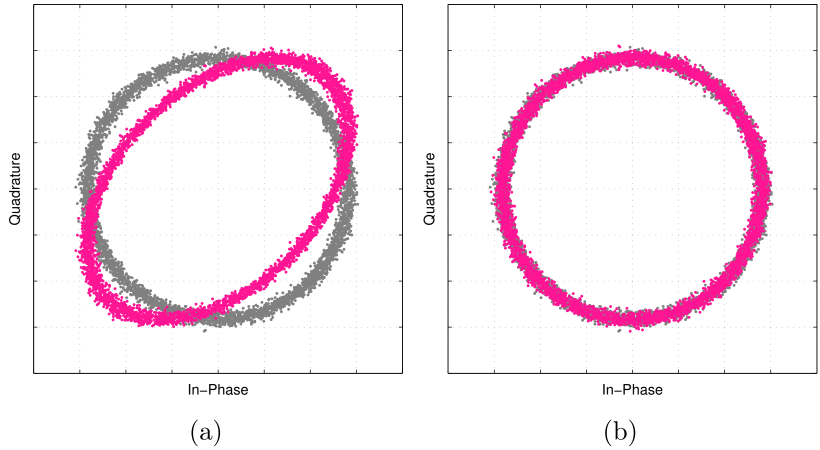

Figure 4.2: Example of a QPSK signal with a remaining IF and (a) $\theta = 25°$ in the 90° hybrid (pink) and (b) the signal after Gram-Schmidt orthogonalization (pink). The gray signal shows the ideal signal with $\theta = 0°$.

$$Q_{\text{orthogonal}}(t) = \frac{Q'(t)}{\sqrt{P_Q}}, \tag{4.5}$$

where $P_I = \langle r_I^2 \rangle$ and $P_Q = \langle r_Q^2 \rangle$ [53, 138]. An example of QPSK with a remaining IF tone and $\theta = 25°$ error in the 90° hybrid is shown in Fig. 4.2a. In this case θ has been exaggerated for illustrative reasons. In Fig. 4.2b, the QPSK signal after Gram-Schmidt orthogonalization is shown.

It should be noted that other orthogonalization algorithms exist such as the Löwdin algorithm which rotates all signal components (compared to Gram-Schmidt which leaves one vector as it is) and creates an orthogonal set of vectors which are closest in least square distance sense to the original set of vectors [139]. The Gram-Schmidt algorithm is simple and has been shown to perform well in QPSK [140] and 16QAM [141] systems. However, with this algorithm quantization noise is added to the transformed component while as for other symmetric methods such as Löwdin algorithm, the quantization noise is equally distributed over both components [53]. Due to this, symmetric methods may be preferred when higher order modulation is used.

It should be noted that impairments in the transmitter that causes non-orthogonal signals are not possible to mitigate in this stage of the DSP using these orthogonalization methods since the I- and Q-components are rotating due to the IF from LO and the polarization state is rotated.

4.2 Low-Pass Filtering and Resampling

In an experiment, it is not uncommon that the ADCs have larger bandwidths than what is needed for the received signal, although this is an unlikely case in a commercial system. The main function of the low-pass filter in the DSP is to suppress noise that is out of band. The bandwidth of the low-pass filter in the DSP relative to the signal symbol rate is a trade-off between noise suppression and the induced intersymbol interference (ISI), but typical values are around 70–75 % of the signal symbol rate. The filter shape is typically a 5th order Bessel filter [142], which has been used throughout this thesis, or 5th order super-Gaussian [143]. In a commercial system the low-pass filtering might not be needed in the DSP since the ADCs and/or the optical hardware in the receiver most likely have a bandwidth lower or close to the symbol rate.

In the same way, for a commercial system the sampling rate of the ADCs would most likely be 2 samples/symbol. However, in an experimental environment the ADCs have limited steps of sampling rates and situations can arise where sample rate is even higher. Down-sampling of the signal to 2 samples/symbol is then performed in the DSP.

4.3 Electronic Dispersion Compensation

With coherent detection, the dispersion compensation can be moved from the optical domain to DSP, which is often referred to as electronic dispersion compensation (EDC). With EDC the DCFs, including the extra EDFAs that often accompany DCFs, can be removed from the system. This can possibly lead to a reduced cost and complexity of the system, though it should be noted that in the optical domain the dispersion for all WDM channels is compensated using a single module, while with DSP the dispersion compensation has to be performed for each channel. The two main benefits on signal quality of EDC are that the nonlinear effects in the transmission system can be reduced, allowing higher launch powers and thus the transmission reach can be increased significantly [144–146] and that the loss in the DCFs is removed. Increased nonlinear tolerance can also be achieved by optically compensating for all the accumulated dispersion at the receiver, or pre-compensating in the transmitter. However, this approach is inflexible and most likely not suited for a fiber network where the signals can be routed differently.

Some of the nonlinear distortions in a periodically compensated link originate from the DCFs, which has a significantly higher nonlinear coefficient compared to standard monomode fiber (SMF). Using chirped fiber-Bragg gratings for dispersion compensation, which themselves do not induce any nonlinear distortion, has been shown as a possible alternative to DCFs [147]. However, inline compensation, even when the dispersion compensation units do not have any nonlinear effects, will still induce more nonlinear impairments compared to an uncompensated case [146].

The chromatic dispersion that an optical signal $A(z,t)$ is impaired with during propagation is described by

$$\frac{\partial A(z,t)}{\partial z} = j\frac{D\lambda^2}{4\pi c}\frac{\partial^2 A(z,t)}{\partial t^2}, \tag{4.6}$$

where D is the dispersion parameter. This equation can be solved in the frequency domain to obtained the dispersion transfer function as

$$H(z,\omega) = \exp\left(-j\frac{D\lambda^2 z}{4\pi c}\omega^2\right), \tag{4.7}$$

which can be transformed back to the time domain as

$$h(z,t) = \sqrt{\frac{c}{jD\lambda^2 z}}\exp\left(j\frac{\pi c}{D\lambda^2 z}t^2\right). \tag{4.8}$$

The chromatic dispersion can then be compensated by applying the inverse of the transfer function $H(z,\omega)$.

To compensate for the dispersion in the time domain, a finite impulse response (FIR) filter is used where the filter taps are given by

$$h_n = \sqrt{\frac{jcT_{samp}^2}{D\lambda^2 L}}\exp\left(-j\frac{\pi c T_{samp}^2}{D\lambda^2 L}n^2\right), \tag{4.9}$$

for $n \in [-N/2, -N/2+1, \ldots, N/2]$. T_{samp} is the sampling interval, L is the transmission distance and N is the number of taps which is dependent on the amount of dispersion that the signal has been subjected to and can be found from $N = 2\left\lfloor (|D|\lambda^2 L)/(2cT_{samp}^2)\right\rfloor$ [148].

The dispersion compensation filter can also be implemented in the frequency domain where the discrete transfer function is given by

$$h_\omega = \exp\left(j\frac{D\lambda^2}{4\pi c}\omega^2\right), \tag{4.10}$$

where $\omega \in 2\pi/T[-N/2, -N/2+1, \ldots, N/2-1]$.

The biggest difference between the two dispersion compensation methods is the computational complexity. For small amount of accumulated dispersion the time domain method is preferred and for high amount of accumulated dispersion the frequency domain method is preferred [149]. Both methods have been applied in this thesis, most notably in Paper B where transmission distances of over 14,000 km were achieved. This transmission distance corresponded to such high amounts of accumulated dispersion that the time domain filter became too computationally demanding to be implementable.

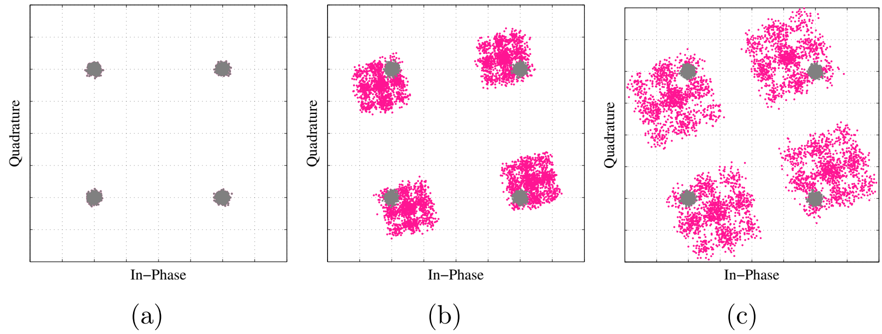

Figure 4.3: Example of increasing amount of dispersion on a 10 Gbaud QPSK signal (pink) and the signal after dispersion compensation has been performed (gray) for no dispersion (a) and increasing amounts in (b) and (c).

Fig. 4.3 shows a QPSK signal with increasing amount of dispersion (pink) as the only impairment and the constellation after dispersion compensation has been applied (gray). For illustrative reasons, a small amount of AWGN has been added to the signal.

4.4 Adaptive Equalization and Polarization Demultiplexing

During transmission, the signal is impaired by different time-varying effects such as rotation of the polarization state and polarization mode dispersion (PMD). These effects are usually compensated for by the use of an adaptive equalizer based on four FIR-filters in a butterfly configuration as shown in Fig. 4.4 [53]. The output of the filter can be expressed as

$$i_{x,out} = \mathbf{h}_{xx}^H \mathbf{i}_x + \mathbf{h}_{xy}^H \mathbf{i}_y, \tag{4.11}$$

$$i_{y,out} = \mathbf{h}_{yy}^H \mathbf{i}_y + \mathbf{h}_{yx}^H \mathbf{i}_x, \tag{4.12}$$

where the filter taps are denoted as $\mathbf{h}_{xx}$, $\mathbf{h}_{xy}$, $\mathbf{h}_{yy}$, $\mathbf{h}_{yx}$. Further, $\mathbf{i}_x$ and $\mathbf{i}_y$ are the sampled complex signals for the x- and y-polarizations. This filter configuration also approximates a matched filter which can mitigate time-invariant impairments such as ISI and residual chromatic dispersion from the EDC [54, Chapter 5.2.1.5]. The optimization of the filter taps is done differently depending on what modulation format that is used. In this section, the optimization of the filters for the modulation formats used in papers A, B and C will be

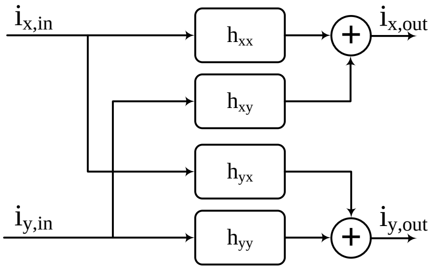

Figure 4.4: Butterfly configuration with four FIR-filters for adaptive equalization.

discussed, namely PM-QPSK, PS-QPSK, 4FPS-QPSK, PM-16QAM and 128-SP-QAM.

4.4.1 Different Modifications of the Constant Modulus Algorithm

To update the filter taps for QPSK the constant modulus algorithm (CMA), first introduced by Godard in 1980 [150], is almost exclusively used. It has later been adapted to polarization diverse optical communication systems where polarization demultiplexing is required [151]. The CMA uses the fact that the QPSK symbols have a constant power, which is also why the CMA can be used before frequency and phase offsets have been compensated. The updating rules for the CMA are

$$\mathbf{h}_{xx} = \mathbf{h}_{xx} - \mu(|i_{x,out}|^2 - P)i_{x,out}\mathbf{i}_x^*, \tag{4.13}$$

$$\mathbf{h}_{xy} = \mathbf{h}_{xy} - \mu(|i_{x,out}|^2 - P)i_{x,out}\mathbf{i}_y^*, \tag{4.14}$$

$$\mathbf{h}_{yx} = \mathbf{h}_{yx} - \mu(|i_{y,out}|^2 - P)i_{y,out}\mathbf{i}_x^*, \tag{4.15}$$

$$\mathbf{h}_{yy} = \mathbf{h}_{yy} - \mu(|i_{y,out}|^2 - P)i_{y,out}\mathbf{i}_y^*, \tag{4.16}$$

where P is the symbol power and μ is the step-size. The magnitude of μ is a tradeoff between convergence time and equalizer performance.

PS-QPSK

The CMA does not work for PS-QPSK since the criterion of constant modulus is not suitable for achieving polarization demultiplexing of PS-QPSK [97]. Instead a modified version of the CMA, often referred to as polarization-switched

CMA (PS-CMA), can be used where the update of the filter taps is done according to

$$\mathbf{h}_{xx} = \mathbf{h}_{xx} - \mu(|i_{x,out}|^2 + 2|i_{y,out}|^2 - P)i_{x,out}\mathbf{i}_x^*, \tag{4.17}$$

$$\mathbf{h}_{xy} = \mathbf{h}_{xy} - \mu(|i_{x,out}|^2 + 2|i_{y,out}|^2 - P)i_{x,out}\mathbf{i}_y^*, \tag{4.18}$$

$$\mathbf{h}_{yx} = \mathbf{h}_{yx} - \mu(|i_{y,out}|^2 + 2|i_{x,out}|^2 - P)i_{y,out}\mathbf{i}_y^*, \tag{4.19}$$

$$\mathbf{h}_{yy} = \mathbf{h}_{yy} - \mu(|i_{y,out}|^2 + 2|i_{x,out}|^2 - P)i_{y,out}\mathbf{i}_y^*. \tag{4.20}$$

The PS-CMA has been shown to have similar performance in terms of convergence and tracking as the CMA for PM-QPSK [97].

4FPS-QPSK

Unfortunately, neither the standard CMA nor the PS-CMA can be used for 4FPS-QPSK due to the fact that on average half of the bit slots has no power, which results in that the equalizer taps do not converge. In paper B, a modified version of PS-CMA was used for adaptive equalization and polarization demultiplexing where a power threshold determines if the equalizer taps should be updated or not. The power of the samples in the two polarizations are calculated as

$$P_x = |i_{x,out}|^2, \tag{4.21}$$

$$P_y = |i_{y,out}|^2. \tag{4.22}$$

If both $P_x < P_{th}$ and $P_y < P_{th}$, where P_{th} is the power threshold, the filter taps are not updated and otherwise the update of the filter taps is done according to the PS-CMA described in equations (4.17)–(4.20).

In paper B, it was found that this adaptive equalizer is sensitive to the input polarization state and also require a smaller step-size, μ, and longer convergence time compared to the PS-CMA. It is generally a disadvantage to use decisions in a blind equalizer and it was found that the equalizer convergence was sensitive to how P_{th} was selected. A possible solution would be to not use a blind equalizer but instead use a data-aided equalizer based on training sequences [109, 110, 152, 153] which would also aid in resolving the phase- and polarization-ambiguities for the two wavelengths. However, the drawback would then be lower SE due to the overhead introduced by the training sequences.

2PPM-QPSK

In the same way as for 4FPS-QPSK, the conventional CMA does not work for 2PPM-QPSK and a modified version of the CMA has to be used to properly equalize and demultiplex the polarizations. For this format, the equalizer taps are updated as

$$\mathbf{h}_{xx} = \mathbf{h}_{xx} - \mu(|i_{x,out}|^2 - P_{0x})i_{x,out}\mathbf{i}_x^*, \tag{4.23}$$

$$\mathbf{h}_{xy} = \mathbf{h}_{xy} - \mu(|i_{x,out}|^2 - P_{0x})i_{x,out}\mathbf{i}_y^*, \tag{4.24}$$

$$\mathbf{h}_{yx} = \mathbf{h}_{yx} - \mu(|i_{y,out}|^2 - P_{0y})i_{y,out}\mathbf{i}_x^*, \tag{4.25}$$

$$\mathbf{h}_{yy} = \mathbf{h}_{yy} - \mu(|i_{y,out}|^2 - P_{0y})i_{y,out}\mathbf{i}_y^*, \tag{4.26}$$

where $P_{0x} = P_0$ when $P_x \geq P_{th}$ and $P_{0x} = 0$ when $P_x < P_{th}$, $P_{0y} = P_0$ when $P_y \geq P_{th}$ and $P_{0y} = 0$ when $P_y < P_{th}$, where P_x and P_y are found by equations (4.21) and (4.22), respectively. As discussed for 4FPS-QPSK, this format could also benefit from the use of data-aided training sequences.

4.4.2 Decision-Directed Least Mean Square Equalizer

The CMA does actually work for equalization and polarization demultiplexing of PM-16QAM, which can seem surprising since the PM-16QAM signal does not have a constant modulus [154]. However, the performance is suboptimal and requires long convergence times [155].

Instead, a decision-directed equalizer is typically used and the CMA is used for pre-convergence of the filter taps [154]. The reason for using CMA initially is that decision-directed equalizers need to operate on a signal that is somewhat close to the transmitted signal so that decisions can be made with reasonably low error probability. In the work of this thesis, a decision-directed least mean square (DD-LMS) algorithm with CMA for pre-convergence has been used. It should be noted that many other equalization methods exist such as the radius-directed equalizer [156] and independent component analysis [157].

The filter taps for the DD-LMS are updated as

$$\mathbf{h}_{xx} = \mathbf{h}_{xx} + \mu(d_x - i_{x,out})\mathbf{i}_x^*, \tag{4.27}$$

$$\mathbf{h}_{xy} = \mathbf{h}_{xy} + \mu(d_x - i_{x,out})\mathbf{i}_y^*, \tag{4.28}$$

$$\mathbf{h}_{yx} = \mathbf{h}_{yx} + \mu(d_y - i_{y,out})\mathbf{i}_x^*, \tag{4.29}$$

$$\mathbf{h}_{yy} = \mathbf{h}_{yy} + \mu(d_y - i_{y,out})\mathbf{i}_y^*, \tag{4.30}$$

where d_x is the symbol closest to $i_{x,out}$ and d_y to $i_{y,out}$. It should be noted that DD-LMS requires frequency and phase offset tracking (described in section 4.5.3), which are performed within the DD-LMS loop.

In Paper A, the DD-LMS in combination with CMA is used for polarization demultiplexing and adaptive equalization for both PM-16QAM and 128-SP-QAM signals with no extra penalty. It is interesting to note that the equalizer considers the signals in the x- and y-polarizations separately and uses the same decisions as for PM-16QAM. It is not obvious that a PM-16QAM equalizer would be functional for 128-SP-QAM which is a subset of PM-16QAM. For instance, for PS-QPSK which is a subset of PM-QPSK, the CMA cannot be used, which is discussed in section 4.4.1. That the same equalization method works for both PM-16QAM and 128-SP-QAM has also been found in [113].

4.5 Frequency and Carrier Phase Estimation

In a coherent receiver with a free-running LO, the transmitter laser and the LO laser will have different center frequencies, which causes the signal to be down-converted to an intermediate frequency rather than to base-band. The intermediate frequency is given by $\omega_{IF} = \omega_s - \omega_{LO}$, where ω_s is the signal angular frequency and ω_{LO} the LO angular frequency. Furthermore, both the transmitter and the LO lasers have phase noise that is of a stochastic nature and is often expressed as the laser linewidth which is related to how long time the phase of the laser is stable. The sampled complex signal can be described as

$$i_x(k) = c_k \exp\left[j(\omega_{IF} kT + \varphi(k)\right], \tag{4.31}$$

where c_k are symbols from the constellation. The phase variation of the symbols is divided into the IF part and the random phase noise part [158].

In principle, a joint phase and frequency estimation can be performed. However this is often unpractical, especially if ω_{IF} is large. Further, the phase estimation schemes are often biased if a frequency offset is present [53] and the performance of the tracking can be increased by first removing the IF. Thus, in the following sections separate IF estimation and phase estimation are considered.

4.5.1 FFT-based Frequency Offset Estimation

In papers A–C, frequency offset estimation based on the fast Fourier transform (FFT) was used. This is done by finding the angular frequency corresponding to the strongest peak in the spectrum of the signal, i.e.,

$$\hat{\omega}_{IF} = \frac{1}{M} \operatorname*{argmax}_{\omega} \{|\mathrm{FFT}(\mathbf{i}_x^M)|^2\}, \tag{4.32}$$

where M is dependent on which modulation format that is used, e.g. $M = 4$ for QPSK [159]. Further, $\mathbf{i}_x$ denotes a set of complex samples.

The same method can be used for QAM formats, but longer batches of samples are then typically required to get an accurate estimate. This makes the linewidth requirements on the transmitter and LO lasers more stringent [154]. This method has been used for both PM-16QAM and 128-SP-QAM in paper A. It should be noted that more efficient methods exist for 16QAM, such as radius-partitioning of the detected symbols before the frequency estimation [160].

To track the random phase fluctuations due to the linewidth of the lasers, $\varphi(k)$ in equation (4.31), different methods are used depending on modulation format. In the following section the Viterbi-Viterbi algorithm is discussed which is typically used for QPSK-based and the blind phase estimation which is used for QAM constellations is discussed in section 4.5.3.

4.5.2 Phase Estimation based on Viterbi-Viterbi

For QPSK, methods based on the Viterbi-Viterbi algorithm [161] are almost exclusively used for carrier phase estimation. QPSK has the nice feature that by raising the signal to the 4th power, the modulation is removed, rotating the four constellation points into a single point [53]. This can also be generalized for M-ary PSK, where the signal should be raised to the M-th power [161]. Using QPSK, the phase can be estimated as

$$\hat{\varphi}(k) = \frac{1}{4} \arg \left\{ \sum_{n=-N}^{N} w(n) i_p^4(k+n) \right\}, \tag{4.33}$$

where $i_p = i_x$ or i_y is the signal in one of the polarizations and $w(n)$ is a weighting function, which can be optimized depending on the SNR (assuming AWGN) [53, 149]. Applying $w(n)$ as a Wiener filter has been shown to achieve performance close to the maximum a posteriori estimate [162] and using $w(n) = 1$ gives one of the original estimates proposed by Viterbi and Viterbi [161].

It should be noted that phase unwrapping is required, or otherwise the tracking is constrained since the output of equation (4.33) is limited to $[-\pi/4, \pi/4]$ [163]. This algorithm can be applied blockwise or using a sliding window, where the later has better performance but is more computationally demanding.

In equation (4.33) the phase is tracked individually in the two polarizations. The Viterbi-Viterbi estimator can be extended to a joint-polarization estimator [164], obviously assuming the same signal laser is used for both polarization states. For PS-QPSK, joint-polarization methods can increase the linewidth tolerance significantly [165]. The Viterbi-Viterbi algorithm was also used for 4FPS-QPSK in paper B, however joint estimation over two carriers was not possible since the lasers were free-running.

4.5.3 Carrier Phase Estimation for QAM Constellations

For QAM constellations the modulation cannot be removed by a single Mth power operation and thus the Viterbi-Viterbi is suboptimal and other methods are preferred. An example of such a method is QPSK-partitioning of the 16QAM constellation to be able to use the Viterbi-Viterbi estimation on different partitions of the 16QAM constellation with constant amplitudes [155, 160, 166].

In paper A, a method based on blind search with different test phases are used for both PM-16QAM and 128-SP-QAM [86]. The test angles are given as

$$\varphi_b = \frac{b\pi}{2B}, \tag{4.34}$$

where B is the number of total test phases and $b = 0, 1, \ldots, B-1$. The squared distance to the closest constellation point $\hat{d}_{k,b}$ is then calculated as

$$|D_{k,b}|^2 = |i_{p,k} \exp(j\varphi_b) - \hat{d}_{k,b}|^2. \tag{4.35}$$

Further, $2N+1$ consecutive test symbols that are rotated by the same φ_b are summed as

$$|s_{k,b}|^2 = \sum_{n=-N}^{N} |D_{k-n,b}|^2. \tag{4.36}$$

The estimated test phase is then found by choosing b such that $|s_{k,b}|^2$ is minimized. Choosing the number of test phases, B, is a tradeoff between computational complexity and accuracy in terms of quantization noise in the estimation. In paper A, $B = 64$ was used.

Chapter 5

Future Outlook

The demand for bandwidth in optical communication systems has been growing exponentially and the supporting technology has kept up with the demand [167]. Of course the data throughput in a single fiber cannot grow exponentially forever, in the end the laws of physics will be limiting. In the past new technologies, such as polarization-multiplexing, the EDFA which enabled WDM and lately merging these technologies with the more sensitive and spectrally efficient coherent systems, could be adapted as the demand was increasing. When the bandwidth supported by the optical fiber and the optical amplifiers is completely filled, other methods have to be used to increase the overall transmission capacity.

A possible solution is the use of spatial division multiplexing [168] using multimode fibers [169], multi-core fibers with low crosstalk [170], multi-core fibers with coupled cores [171], multi-core fibers where the cores can be multimode [172] or multi-element fibers where the different cores have individual claddings [173]. An interesting approach would be to investigate different multidimensional modulation formats, for instance those suggested in paper D, for these types of fibers. To perform multiple input multiple output (MIMO) processing to suppress crosstalk between cores or modes, different wavelengths have to be routed to the same receiver and therefore modulation formats over several cores/modes using the same wavelength could be considered. These types of fibers also open up new possibilities such as self-homodyne systems where a pilot-tone is transmitted in one of the cores and is used as a phase reference in the receiver [174].

The modulation formats in papers A–C and to some extent paper D could possibly be utilized for a modulation format-flexible system with blind receiver algorithms similar to [108, 109]. However, substantial work on a format-independent equalizer and a flexible transmitter structure would have to be developed, since for instance the same CMA structure cannot be used for both PM-QPSK and PS-QPSK [97].

All formats considered in this thesis suffer from phase and polarization ambiguities due to blind phase estimation. To investigate data-aided training sequences, similar to what was done in [108, 123, 128, 152], would be highly interesting since not only would it resolve the ambiguities but could also be utilized to aid all parts of the DSP.

Finally, all modulation formats can be expressed as codes on other formats. For instance, QPSK could be expressed as a crude code on 16QAM and 128-SP-QAM is a single-parity check code applied to PM-16QAM. Co-optimization of codes and modulation formats would be of great interest as little is done on this subject, often referred to as coded-modulation [92], for the nonlinear fiber channel. The days of hard-decoded FEC based on Reed-Solomon codes [175] could be over for the fiber optical systems as more advanced codes are starting to be used, for instance in [116] LDPC codes with 28% overhead were used. Codes that are optimized for nonlinear transmission have the possibility to greatly outperform today's systems where codes and modulation formats are treated separately.

Chapter 6

Summary of Papers

Paper A

"Comparison of 128-SP-QAM and PM-16QAM in Long-haul WDM Transmission", *Optics Express*, vol. 21, no. 16, pp. 19269-19279, 2013.

In this paper we experimentally investigate 128-ary set-partitioning quadrature amplitude modulation (128-SP-QAM) which is a subset of PM-16QAM. We investigated the back-to-back sensitivity gain of 128-SP-QAM and compared the results to PM-16QAM both at the same symbol rate and bit rate. The two formats are compared in both single channel and wavelength-division multiplexed transmission. We show that the maximum transmission reach can be increased by 50% by going to 128-SP-QAM to PM-16QAM, compared at the same bit rate.

Paper B

"Frequency and Polarization Switched QPSK", *European Conference and Exhibition on Optical Communication (ECOC)*, London, England, paper Th.2.D.4, 2013.

Much research, both theoretical and experimental, has been devoted to 4-dimensional modulation formats. In this paper we explore the possibilities of going to 8 dimensions by considering two neighboring wavelength channels as one signal. We experimentally implement biorthogonal modulation in 8 dimensions which for each symbol transmits one QPSK signal in one of the four possible slots given by the two polarization states of the two wavelengths. Due to this implementation we designate the format 4-ary frequency and polarization switched QPSK (4FPS-QPSK). This format has 3 dB increased asymptotic power efficiency over QPSK at the cost of half spectral efficiency. We compare this format to dual-carrier (DC) PM-QPSK and DC polarization-switched QPSK at the same symbol rate and we detect the two wavelength channels using a single coherent receiver. We show a 4.2 dB increased back-to-back sensitivity for 4FPS-QPSK over DC-PM-QPSK and transmission of 4FPS-QPSK of up to 14,000 km which was an increase of 84 % over DC-PM-QPSK.

Paper C

"Long-Haul Transmission of PM-2PPM-QPSK at 42.8 Gbit/s", *Optical Fiber Communication Conference (OFC)*, Anaheim, USA, paper OTu2B.7, 2013.

Polarization-switched QPSK (PS-QPSK) is the most power efficient modulation format in 4 dimensions and has attracted a lot of research interest for coherent fiber optical systems. In this paper we experimentally investigate binary pulse position modulation QPSK (2PPM-QPSK) which is a modulation format with the same spectral efficiency and asymptotic power efficiency as PS-QPSK. Instead of transmitting a QPSK symbol in either the x- or y-polarization as for PS-QPSK, 2PPM-QPSK transmits one QPSK in either of two neighboring time slots. In this paper we show the first experimental realization of PM-2PPM-QPSK and compare the performance to PM-QPSK at the same bit rate. We show that the transmission distance can be increased by approximately 40 % by using PM-2PPM-QPSK over PM-QPSK compared at the same bit rate.

Paper D

"K-over-L Multidimensional Position Modulation", Submitted to *IEEE Journal of Lightwave Technology*, September 2013; revised, January 2014.

In this theoretical paper we analyze a family of modulation formats based on multidimensional position modulation (MDPM) which is a generalization of pulse position modulation (PPM). For MDPM, the different slots can be realized by different time slots, polarization states, wavelength channels, different modes of a multimode fiber, different cores of a multicore fiber or any combination of these. We show that by using multiple pulses per frame, K-over-L-MDPM, in combination with QPSK it is possible to simultaneously increase both the spectral efficiency and the asymptotic power efficiency over conventional QPSK. We identify K-ary inverse-MDPM (KiMDPM), the special case of K-over-(K–1)-MDPM, as practically interesting modulation formats since they carry an integer number of bits per frame when K is a power of two. We show that 4iMDPM-QPSK has a 1.25 dB increased asymptotic power efficiency over QPSK with a maintained spectral efficiency. We also investigate 4iMDPM-QPSK and 8iMDPM-QPSK in the low SNR regime by Monte Carlo simulations with additive white Gaussian noise as the only impairment and show that the sensitivity of 4iMDPM-QPSK is better compared to QPSK for bit-error probabilities lower than 8.3×10^{-3}.

References

[1] Digital Cinema Initiatives, LLC, "Digital cinema system specification version 1.2 with errata as of 30 August 2012 incorporated," 2012.

[2] ITU-R, "Parameter values for ultra-high definition television systems for production and international programme exchange," ITU-R BT.2020, 2012.

[3] M. N. Sadiku, S. M. Musa, and O. D. Momoh, "Cloud computing: Opportunities and challenges," *IEEE Potentials*, vol. 33, no. 1, pp. 34–36, 2014.

[4] ITU World Telecommunication/ICT Indicators database, "Internet users per 100 inhabitants, 2001-2011," 2011.

[5] ITU World Telecommunication/ICT Indicators database, "Key ICT indicators for developed and developing countries and the world (totals and penetration rates)," 2013.

[6] T. H. Maiman, "Stimulated optical radiation in ruby," *Nature*, vol. 187, pp. 493–494, Aug. 1960.

[7] R. Hall, G. Fenner, J. Kingsley, T. Soltys, and R. Carlson, "Coherent light emission from GaAs junctions," *Physical Review Letters*, vol. 9, no. 9, pp. 366–368, 1962.

[8] M. I. Nathan, W. P. Dumke, G. Burns, F. H. Dill, and G. Lasher, "Stimulated emission of radiation from GaAs p-n junctions," *Applied Physics Letters*, vol. 1, no. 3, p. 62, 1962.

[9] K. Kao and G. Hockham, "Dielectric-fibre surface waveguides for optical frequencies," *Proceedings of the Institution of Electrical Engineers*, vol. 113, no. 7, p. 1151, 1966.

[10] F. P. Kapron, D. B. Keck, and R. D. Maurer, "Radiation losses in glass optical waveguides," *Applied Physics Letters*, vol. 17, no. 10, p. 423, 1970.

[11] D. Keck, R. Maurer, and P. Schultz, "On the ultimate lower limit of attenuation in glass optical waveguides," *Applied Physics Letters*, vol. 22, no. 7, p. 307, 1973.

[12] M. Horiguchi and H. Osanai, "Spectral losses of low-OH-content optical fibres," *Electronics Letters*, vol. 12, no. 12, pp. 310–312, 1976.

[13] K. Nagayama, M. Kakui, M. Matsui, T. Saitoh, and Y. Chigusa, "Ultra-low-loss (0.1484 dB/km) pure silica core fibre and extension of transmission distance," *Electronics Letters*, vol. 38, no. 20, pp. 1168–1169, 2002.

[14] M. Hirano, T. Haruna, Y. Tamura, T. Kawano, S. Ohnuki, Y. Yamamoto, Y. Koyano, and T. Sasaki, "Record low loss, record high FOM optical fiber with manufacturable process," in *Optical Fiber Communication Conference (OFC)*, p. PDP5A.7., 2013.

[15] S. Personick, "Receiver design for digital fiber optic communication systems, I & II," *Bell System Technical Journal*, 1973.

[16] J. Hecht, *City of Light: The Story of Fiber Optics.* Oxford University Press, 199.

[17] H. Osanai, T. Shioda, T. Moriyama, S. Araki, M. Horiguchi, T. Izawa, and H. Takata, "Effect of dopants on transmission loss of low-OH-content optical fibres," *Electronics Letters*, vol. 12, no. 21, pp. 549–550, 1976.

[18] D. Payne and W. Gambling, "Zero material dispersion in optical fibres," *Electronics Letters*, vol. 11, no. 8, pp. 176 – 178, 1975.

[19] R. S. Kerdock and D. H. Wolaver, "Atlanta fiber system experiment: Results of the Atlanta experiment," *Bell System Technical Journal*, vol. 57, no. 6, pp. 1857–1879, 1978.

[20] A. H. Gnauck, R. Tkach, A. Chraplyvy, and T. Li, "High-capacity optical transmission systems," *Journal of Lightwave Technology*, vol. 26, no. 9, pp. 1032–1045, 2008.

[21] "AT&T learns how to cope with sharks," *Toledo Blade*, p. 6, Aug. 30 1987.

[22] S. Abbott, “Review of 20 years of undersea optical fiber transmission system development and deployment since TAT-8,” in *European Conference and Exhibition on Optical Communication (ECOC)*, p. Mo.4.E.1, 2008.

[23] B. Glance, “Polarization independent coherent optical receiver,” *Journal of Lightwave Technology*, vol. 5, no. 2, pp. 274–276, 1987.

[24] S. Poole, D. Payne, and M. Fermann, “Fabrication of low-loss optical fibres containing rare-earth ions,” *Electronics Letters*, vol. 21, no. 17, pp. 737–738, 1985.

[25] R. Mears, L. Reekie, I. Jauncey, D. Payne, C. B. Morrison, D. Botez, L. M. Zinkiewicz, O. S. Park, and R. Beach, “Low-noise erbium-doped fibre amplifier operating at 1.54μm,” *Electronics Letters*, vol. 23, no. 19, pp. 1026–1028, 1987.

[26] H. Taga, Y. Yoshida, N. Edagawa, S. Yamamoto, and H. Wakabayashi, “459 km, 2.4 Gbit/s four wavelength multiplexing optical fibre transmission experiment using six Er-doped fibre amplifiers,” *Electronics Letters*, vol. 26, no. 8, pp. 500–501, 1990.

[27] N. S. Bergano, J. Aspell, C. R. Davidson, P. R. Trischitta, B. M. Nyman, and F. W. Kerfoot, “A 9000 km 5 Gb/s and 21,000 km 2.4 Gb/s feasibility demonstration of transoceanic EDFA systems using a circulating loop,” in *Optical Fiber Communication Conference (OFC)*, vol. 4, (San Diego, California), p. PD13, 1991.

[28] K. Inoue, “Four-wave mixing in an optical fiber in the zero-dispersion wavelength region,” *Journal of Lightwave Technology*, vol. 10, no. 11, pp. 1553–1561, 1992.

[29] A. Chraplyvy, A. Gnauck, R. Tkach, and R. Derosier, “8 $\times$ 10 Gb/s transmission through 280 km of dispersion-managed fiber,” *IEEE Photonics Technology Letters*, vol. 5, no. 10, pp. 1233–1235, 1993.

[30] A. J. Antos and D. K. Smith, “Design and characterization of dispersion compensating fiber based on the LP_{01} mode,” *Journal of Lightwave Technology*, vol. 12, no. 10, pp. 1739–1745, 1994.

[31] A. M. Vengsarkar, A. E. Miler, and W. A. Reed, “Highly efficient single-mode fiber for broadband dispersion compensation,” in *Optical Fiber Communication Conference (OFC)*, vol. 4, (San Jose, California), p. PD13, 1993.

[32] S. Kawakami and S. Nishida, "Characteristics of a doubly clad optical fiber with a low-index inner cladding," *IEEE Journal of Quantum Electronics*, vol. 10, no. 12, pp. 879–887, 1974.

[33] K. Oda, M. Fukutoku, M. Fukui, T. Kitoh, and H. Toba, "16-channel × 10-Gbit/s optical FDM transmission over a 1000 km conventional single-mode fiber employing dispersion-compensating fiber and gain equalization," in *Optical Fiber Communication Conference (OFC)*, p. PD22, 1995.

[34] H. Onaka, H. Miyata, G. Ishikawa, K. Otsuka, H. Ooi, Y. Kai, S. Kinoshita, M. Seino, H. Nishimoto, and T. Chikama, "1.1 Tb/s WDM transmission over a 150 km 1.3 μm zero-dispersion single-mode fiber," in *Optical Fiber Communication Conference (OFC)*, p. PD19, 1996.

[35] T. Pfau, S. Hoffmann, R. Peveling, S. Ibrahim, O. Adamczyk, M. Porrmann, S. Bhandare, R. Noé, and Y. Achiam, "Synchronous QPSK transmission at 1.6 Gbit/s with standard DFB lasers and real-time digital receiver," *Electronics Letters*, vol. 42, no. 20, pp. 1175–1176, 2006.

[36] H. Sun, K.-T. Wu, and K. Roberts, "Real-time measurements of a 40 Gb/s coherent system," *Optics Express*, vol. 16, no. 2, pp. 873–879, 2008.

[37] G. Agrawal, *Fiber-Optic Communication Systems.* Wiley Series in Microwave and Optical Engineering, Wiley, 4th ed., 2012.

[38] M. Islam, "Raman amplifiers for telecommunications," *IEEE Journal of Selected Topics in Quantum Electronics*, vol. 8, no. 3, pp. 548–559, 2002.

[39] L. Spiekman, J. Wiesenfeld, A. Gnauck, L. Garrett, G. Van Den Hoven, T. Van Dongen, M. Sander-Jochem, and J. Binsma, "Transmission of 8 DWDM channels at 20 Gb/s over 160 km of standard fiber using a cascade of semiconductor optical amplifiers," *IEEE Photonics Technology Letters*, vol. 12, no. 6, pp. 717–719, 2000.

[40] Z. Tong, C. Lundström, P. A. Andrekson, C. J. McKinstrie, M. Karlsson, D. J. Blessing, E. Tipsuwannakul, B. J. Puttnam, H. Toda, and L. Grüner-Nielsen, "Towards ultrasensitive optical links enabled by low-noise phase-sensitive amplifiers," *Nature Photonics*, vol. 5, no. 7, pp. 430–436, 2011.

[41] International Telecommunication Union (ITU), "Optical fibres, cables and systems," 2009.

[42] S. Benedetto and E. Biglieri, *Principles of Digital Transmission: With Wireless Applications.* Information Technology Series, Springer, 1999.

[43] J. Proakis and M. Salehi, *Digital Communications.* McGraw-Hill International Edition, McGraw-Hill Higher Education, 5th ed., 2008.

[44] A. Splett, C. Kurtzke, and K. Petermann, "Ultimate transmission capacity of amplified optical fiber communication systems taking into account fiber nonlinearities," in *European Conference and Exhibition on Optical Communication (ECOC)*, p. MoC2.4, 1993.

[45] P. Poggiolini, "The GN model of non-linear propagation in uncompensated coherent optical systems," *Journal of Lightwave Technology*, vol. 30, no. 24, pp. 3857–3879, 2012.

[46] P. Johannisson and M. Karlsson, "Perturbation analysis of nonlinear propagation in a strongly dispersive optical communication system," *Journal of Lightwave Technology*, vol. 31, no. 8, pp. 1273–1282, 2013.

[47] G. Abbas, V. Chan, and T. Yee, "A dual-detector optical heterodyne receiver for local oscillator noise suppression," *Journal of Lightwave Technology*, vol. 3, no. 5, pp. 1110–1122, 1985.

[48] F. Favre, L. U. C. Jeunhomme, I. Joindot, M. Monerie, and J. C. J. Simon, "Progress towards heterodyne-type single-mode fiber communication systems," *IEEE Journal of Quantum Electronics*, vol. 17, no. 6, pp. 897–906, 1981.

[49] E. Desurvire, J. R. Simpson, and P. C. Becker, "High-gain erbium-doped traveling-wave fiber amplifier," *Optics Letters*, vol. 12, no. 11, pp. 888–890, 1987.

[50] K. Roberts, "Electronic dispersion compensation beyond 10 Gb/s," in *IEEE/LEOS Summer Topical Meetings 2007*, p. MA2.3, 2007.

[51] T. Pfau, S. Hoffmann, O. Adamczyk, R. Peveling, V. Herath, M. Porrmann, and R. Noé, "Coherent optical communication: Towards realtime systems at 40 Gbit/s and beyond," *Optics Express*, vol. 16, no. 2, pp. 873–879, 2008.

[52] M. Seimetz and C.-M. Weinert, "Options, feasibility, and availability of 2×4 90° hybrids for coherent optical systems," *Journal of Lightwave Technology*, vol. 24, no. 3, pp. 1317–1322, 2006.

[53] S. J. Savory, "Digital coherent optical receivers: Algorithms and subsystems," *IEEE Journal of Selected Topics in Quantum Electronics*, vol. 16, pp. 1164–1179, Sept. 2010.

[54] I. Kaminow, T. Li, and A. Willner, *Optical Fiber Telecommunications Volume VIB: Systems and Networks.* Elsevier Science, 2013.

[55] "IEEE trial-use standard for digitizing waveform recorders," IEEE Std 1057, 1989.

[56] C. Vogel and H. Johansson, "Time-interleaved analog-to-digital converters: Status and future directions," in *IEEE International Symposium on Circuits and Systems 2006*, pp. 3386–3389, 2006.

[57] J. K. Fischer, R. Ludwig, L. Molle, C. Schmidt-Langhorst, C. C. Leonhardt, A. Matiss, and C. Schubert, "High-speed digital coherent receiver based on parallel optical sampling," *Journal of Lightwave Technology*, vol. 29, no. 4, pp. 378–385, 2011.

[58] K. Okamoto and F. Ito, "Dual-channel linear optical sampling for simultaneously monitoring ultrafast intensity and phase modulation," *Journal of Lightwave Technology*, vol. 27, no. 12, pp. 2169–2175, 2009.

[59] F. X. Kärtner, R. Amatya, M. Araghchini, J. Birge, H. Byun, J. Chen, M. Dahlem, N. A. DiLello, F. Gan, C. W. Holzwarth, J. L. Hoyt, E. P. Ippen, A. Khilo, J. Kim, M. Kim, A. Motamedi, J. S. Orcutt, M. Park, M. Perrott, M. A. Popović, R. J. Ram, H. I. Smith, G. R. Zhou, S. J. Spector, T. M. Lyszczarz, M. W. Geis, D. M. Lennon, J. U. Yoon, M. E. Grein, and R. T. Schulein, "Photonic analog-to-digital conversion with electronic-photonic integrated circuits," in *SPIE Photonics West 2008*, 2008.

[60] A. Khilo, S. J. Spector, M. E. Grein, A. H. Nejadmalayeri, C. W. Holzwarth, M. Y. Sander, M. S. Dahlem, M. Y. Peng, M. W. Geis, N. A. DiLello, J. U. Yoon, A. Motamedi, J. S. Orcutt, J. P. Wang, C. M. Sorace-Agaskar, M. A. Popović, J. Sun, G.-R. Zhou, H. Byun, J. Chen, J. L. Hoyt, H. I. Smith, R. J. Ram, M. Perrott, T. M. Lyszczarz, E. P. Ippen, and F. X. Kärtner, "Photonic ADC: overcoming the bottleneck of electronic jitter," *Optics Express*, vol. 20, no. 4, pp. 4454–4469, 2012.

[61] K. Morito, R. Sahara, K. Sato, and Y. Kotaki, "Penalty-free 10 Gb/s NRZ transmission over 100 km of standard fiber at 1.55 μm with a blue-chirp modulator integrated DFB laser," *IEEE Photonics Technology Letters*, vol. 8, no. 3, pp. 431–433, 1996.

[62] C. Brackett, "Dense wavelength division multiplexing networks: principles and applications," *IEEE Journal on Selected Areas in Communications*, vol. 8, no. 6, pp. 948–964, 1990.

[63] Y. Miyamoto, A. Hirano, K. Yonenaga, A. Sano, H. Toba, K. Murata, and O. Mitomi, “320 Gbit/s (8 × 40 Gbit/s) WDM transmission over 367 km with 120 km repeater spacing using carrier-suppressed return-to-zero format,” *Electronics Letters*, vol. 35, no. 23, p. 2041, 1999.

[64] W. Bogner, E. Gottwald, A. Schöpflin, and C.-J. Weiske, “40 Gbit/s unrepeatered optical transmission over 148 km by electrical time division multiplexing and demultiplexing,” *Electronics Letters*, vol. 33, no. 25, pp. 2136–2137, 1997.

[65] C. Scheerer, C. Glingener, A. Färbert, J.-P. Elbers, A. Schöpflin, E. Gottwald, and G. Fischer, “3.2 Tbit/s (80 × 40 Gbit/s) bidirectional WDM/ETDM transmission over 40 km standard singlemode fibre,” *Electronics Letters*, vol. 35, no. 20, pp. 1752–1753, 1999.

[66] D. Breuer and K. Petermann, “Comparison of NRZ- and RZ-modulation format for 40-Gb/s TDM standard-fiber systems,” *IEEE Photonics Technology Letters*, vol. 9, no. 3, pp. 398–400, 1997.

[67] M. Nakazawa, T. Yamamoto, and K. R. Tamura, “1.28 Tbit/s-70 km OTDM transmission using third- and fourth-order simultaneous dispersion compensation with a phase modulator,” *Electronics Letters*, vol. 36, no. 24, pp. 2027–2029, 2000.

[68] S. Kawanishi, I. Shake, K. Mori, H. Takara, K. Uchiyama, I. Shake, and K. Mori, “3 Tbit/s (160 Gbit/s × 19 channel) optical TDM and WDM transmission experiment,” *Electronics Letters*, vol. 35, no. 10, p. 826, 1999.

[69] K. Yonenaga and K. Hagimoto, “10-Gbit/s × four-channel WDM transmission experiment over 2400-km DSF using optical DPSK direct detection scheme,” in *Optical Fiber Communication Conference (OFC)*, p. ThS2, 1997.

[70] M. Rohde, C. Caspar, N. Heimes, M. Konitzer, E.-J. Bachus, and N. Hanik, “Robustness of DPSK direct detection transmission format in standard fibre WDM systems,” *Electronics Letters*, vol. 36, no. 17, pp. 1483–1484, 2000.

[71] C. Xu, X. Liu, and X. Wei, “Differential phase-shift keying for high spectral efficiency optical transmissions,” *IEEE Journal of Selected Topics in Quantum Electronics*, vol. 10, no. 2, pp. 281–293, 2004.

[72] E. Tipsuwannakul, P. Johannisson, M. Sköld, E. Agrell, M. Karlsson, and P. A. Andrekson, "Performance comparison of differential 8-ary modulation formats in high-speed optical transmission systems," *Journal of Lightwave Technology*, vol. 29, no. 19, pp. 2954–2962, 2011.

[73] A. H. Gnauck, G. Charlet, P. Tran, P. J. Winzer, C. R. Doerr, J. C. Centanni, E. C. Burrows, T. Kawanishi, T. Sakamoto, and K. Higuma, "25.6-Tb/s WDM transmission of polarization-multiplexed RZ-DQPSK signals," *Journal of Lightwave Technology*, vol. 26, no. 1, pp. 79–84, 2008.

[74] "Coherent DWDM technologies." White Paper, Infinera, 2012.

[75] "6500 packet-optical platform." Datasheet, Ciena, 2011.

[76] E. Agrell and M. Karlsson, "Power-efficient modulation formats in coherent transmission systems," *Journal of Lightwave Technology*, vol. 27, no. 22, pp. 5115–5126, 2009.

[77] F. Gray, "Pulse code communication," 1953. US Patent 2,632,058.

[78] E. Agrell, J. Lassing, E. Ström, and T. Ottosson, "On the optimality of the binary reflected gray code," *IEEE Transactions on Information Theory*, vol. 50, no. 12, pp. 3170–3182, 2004.

[79] M. Ohm and T. Freckmann, "Comparison of different DQPSK transmitters with NRZ and RZ impulse shaping," in *IEEE/LEOS Workshop on Advanced Modulation Formats, 2004*, p. ThB2, IEEE, 2004.

[80] X. Liu, A. R. Chraplyvy, P. J. Winzer, R. W. Tkach, and S. Chandrasekhar, "Phase-conjugated twin waves for communication beyond the Kerr nonlinearity limit," *Nature Photonics*, vol. 7, no. 7, pp. 560–568, 2013.

[81] M. Seimetz, M. Noelle, and E. Patzak, "Optical systems with high-order DPSK and star QAM modulation based on interferometric direct detection," *Journal of Lightwave Technology*, vol. 25, no. 6, pp. 1515–1530, 2007.

[82] C. Doerr, L. Zhang, P. Winzer, and A. Gnauck, "28-Gbaud InP square or hexagonal 16-QAM modulator," in *Optical Fiber Communication Conference (OFC)*, p. OMU2, 2011.

[83] L. Beygi, E. Agrell, and M. Karlsson, "Optimization of 16-point ring constellations in the presence of nonlinear phase noise," in *Optical Fiber Communication Conference (OFC)*, p. OThO4, 2011.

[84] G.-W. Lu, M. Sköld, P. Johannisson, J. Zhao, M. Sjödin, H. Sunnerud, M. Westlund, A. Ellis, and P. A. Andrekson, "40-Gbaud 16-QAM transmitter using tandem IQ modulators with binary driving electronic signals," *Optics Express*, vol. 18, no. 22, pp. 23062–23069, 2010.

[85] T. Sakamoto, A. Chiba, and T. Kawanishi, "50-Gb/s 16 QAM by a quad-parallel Mach-Zehnder modulator," in *European Conference and Exhibition on Optical Communication (ECOC)*, p. PD2.8, 2007.

[86] T. Pfau, S. Hoffmann, and R. Noé, "Hardware-efficient coherent digital receiver concept with feedforward carrier recovery for M-QAM constellations," *Journal of Lightwave Technology*, vol. 27, no. 8, pp. 989–999, 2009.

[87] S. Betti, F. Curti, G. de Marchis, and E. Iannone, "Exploiting fibre optics transmission capacity: 4-quadrature multilevel signalling," *Electronics Letters*, vol. 26, no. 14, p. 992, 1990.

[88] S. Betti, F. Curti, G. D. Marchis, E. Iannone, G. De Marchis, and E. Iannone, "A novel multilevel coherent optical system: 4-quadrature signaling," *Journal of Lightwave Technology*, vol. 9, no. 4, pp. 514–523, 1991.

[89] G. Taricco, E. Biglieri, and V. Castellani, "Applicability of four-dimensional modulations to digital satellites: a simulation study," *European Transactions on Telecommunications*, vol. 6, no. 3, pp. 327–336, 1995.

[90] H. Bülow, "Polarization QAM modulation (POL-QAM) for coherent detection schemes," in *Optical Fiber Communication Conference (OFC)*, p. OWG2, 2009.

[91] M. Karlsson and E. Agrell, "Which is the most power-efficient modulation format in optical links?," *Optics Express*, vol. 17, no. 13, pp. 10814–10819, 2009.

[92] H. Bülow and E. S. Masalkina, "Coded modulation in optical communications," in *Optical Fiber Communication Conference (OFC)*, p. OThO1, 2011.

[93] L. Zetterberg and H. Brändström, "Codes for combined phase and amplitude modulated signals in a four-dimensional space," *IEEE Transactions on Communications*, vol. 25, no. 9, pp. 943–950, 1977.

[94] L. Coelho and N. Hanik, "Global optimization of fiber-optic communication systems using four-dimensional modulation formats," in *European Conference and Exhibition on Optical Communication (ECOC)*, p. Mo.2.B.4, 2011.

[95] G. Ungerboeck, "Channel coding with multilevel / phase signals," *IEEE Transactions on Information Theory*, vol. 28, no. 1, pp. 55–67, 1982.

[96] M. Karlsson and E. Agrell, "Spectrally efficient four-dimensional modulation," in *Optical Fiber Communication Conference (OFC)*, p. OTu2C.1, 2012.

[97] P. Johannisson, M. Sjödin, M. Karlsson, H. Wymeersch, E. Agrell, and P. A. Andrekson, "Modified constant modulus algorithm for polarization-switched QPSK," *Optics Express*, vol. 19, no. 8, pp. 7734–41, 2011.

[98] M. Sjödin, P. Johannisson, H. Wymeersch, P. A. Andrekson, and M. Karlsson, "Comparison of polarization-switched QPSK and polarization-multiplexed QPSK at 30 Gbit/s," *Optics Express*, vol. 19, no. 8, pp. 7839–7846, 2011.

[99] D. S. Millar, D. Lavery, S. Makovejs, C. Behrens, B. C. Thomsen, P. Bayvel, and S. J. Savory, "Generation and long-haul transmission of polarization-switched QPSK at 42.9 Gb/s," *Optics Express*, vol. 19, no. 10, pp. 9296–9302, 2011.

[100] M. Nölle, J. K. Fischer, L. Molle, C. Schmidt-Langhorst, D. Peckham, and C. Schubert, "Comparison of 8 $\times$ 112 Gb/s PS-QPSK and PDM-QPSK signals over transoceanic distances," *Optics Express*, vol. 19, no. 24, pp. 24370–24375, 2011.

[101] D. Lavery, C. Behrens, S. Makovejs, D. S. Millar, R. I. Killey, S. J. Savory, and P. Bayvel, "Long-haul transmission of PS-QPSK at 100 Gb/s using digital backpropagation," *IEEE Photonics Technology Letters*, vol. 24, no. 3, pp. 176–178, 2012.

[102] J. Renaudier, O. Bertran-Pardo, H. Mardoyan, M. Salsi, P. Tran, E. Dutisseuil, G. Charlet, and S. Bigo, "Experimental comparison of 28Gbaud polarization switched- and polarization division multiplexed-QPSK in WDM long-haul transmission system," in *European Conference and Exhibition on Optical Communication (ECOC)*, p. Mo.2.B.3, 2011.

[103] J. K. Fischer, L. Molle, M. Nölle, D.-D. Groß, C. Schmidt-Langhorst, and C. Schubert, "Experimental investigation of 84-Gb/s and 112-Gb/s

polarization-switched quadrature phase- shift keying signals," *Optics Express*, vol. 19, no. 26, pp. B667–B672, 2011.

[104] L. E. Nelson, X. Zhou, N. Mac Suibhne, A. D. Ellis, and P. Magill, "Experimental comparison of coherent polarization-switched QPSK to polarization-multiplexed QPSK for 10 $\times$ 100 km WDM transmission," *Optics Express*, vol. 19, no. 11, pp. 10849–10856, 2011.

[105] "40 Gb/s polarization modulator." Datasheet, Versawave Technologies Inc., 2010.

[106] H. Yamazaki, T. Goh, T. Saida, Y. Hashizume, and S. Mino, "IQ-coupling-loss-free polarization-switched QPSK modulator," in *Optical Fiber Communication Conference (OFC)*, p. PDP5A.8, 2012.

[107] P. Poggiolini, G. Bosco, A. Carena, V. Curri, and F. Forghieri, "Performance evaluation of coherent WDM PS-QPSK (HEXA) accounting for non-linear fiber propagation effects," *Optics Express*, vol. 18, no. 11, pp. 11360–11371, 2010.

[108] J. Fischer, S. Alreesh, R. Elschner, F. Frey, M. Nölle, and C. Schubert, "Bandwidth-variable transceivers based on 4D modulation formats for future flexible networks," in *European Conference and Exhibition on Optical Communication (ECOC)*, p. Tu.3.C.1, 2013.

[109] R. Elschner, F. Frey, C. Meuer, J. K. Fischer, S. Alreesh, C. Schmidt-Langhorst, L. Molle, T. Tanimura, and C. Schubert, "Experimental demonstration of a format-flexible single carrier coherent receiver using data-aided digital signal processing," in *European Conference and Exhibition on Optical Communication (ECOC)*, p. We.1.A.4, 2012.

[110] R. Elschner, F. Frey, C. Meuer, J. K. Fischer, S. Alreesh, C. Schmidt-Langhorst, L. Molle, T. Tanimura, and C. Schubert, "Data-aided digital signal processing for format-flexible transponders," in *Photonic Networks, 14. ITG Symposium*, 2013.

[111] J. Renaudier, A. Voicila, O. Bertran-Pardo, O. Rival, M. Karlsson, G. Charlet, and S. Bigo, "Comparison of set-partitioned two-polarization 16QAM formats with PDM-QPSK and PDM-8QAM for optical transmission systems with error-correction coding," in *European Conference and Exhibition on Optical Communication (ECOC)*, p. We.1.C.5, 2012.

[112] "Digital video broadcasting (DVB) user guidelines for the second generation system for broadcasting, interactive services, news gathering and

other broadband satellite applications (DVB-S2)," Tech. Rep. 102 376 v1.1.1, European Telecommunications Standards Institute, 2005.

[113] M. Sjödin, P. Johannisson, and J. Li, "Comparison of 128-SP-QAM with PM-16-QAM," *Optics Express*, vol. 20, no. 8, pp. 8356–8366, 2012.

[114] T. A. Eriksson, M. Sjödin, P. A. Andrekson, and M. Karlsson, "Experimental demonstration of 128-SP-QAM in uncompensated long-haul transmission," in *Optical Fiber Communication Conference (OFC)*, p. OTu3B.2, 2013.

[115] J. Renaudier, O. Bertran-Pardo, A. Ghazisaeidi, P. Tran, H. Mardoyan, P. Brindel, A. Voicila, G. Charlet, and S. Bigo, "Experimental transmission of Nyquist pulse shaped 4-D coded modulation using dual polarization 16QAM set-partitioning schemes at 28 Gbaud," in *Optical Fiber Communication Conference (OFC)*, p. OTu3B.1, 2013.

[116] H. Zhang, J.-X. Cai, H. G. Batshon, M. Mazurczyk, O. V. Sinkin, D. G. Foursa, A. Pilipetskii, G. Mohs, and N. S. Bergano, "200 Gb/s and dual-wavelength 400 Gb/s transmission over transpacific distance at 6 b/s/Hz spectral efficiency," in *Optical Fiber Communication Conference (OFC)*, p. PDP5A.6., 2013.

[117] H. Sun, R. Egorov, B. E. Basch, J. McNicol, and W. Kuang-Tsan, "Comparison of two modulation formats at spectral efficiency of 5 bits/dual-pol symbol," in *European Conference and Exhibition on Optical Communication (ECOC)*, p. Th.2.D.3., 2013.

[118] M. Karlsson and E. Agrell, "Four-dimensional optimized constellations for coherent optical transmission systems," in *European Conference and Exhibition on Optical Communication (ECOC)*, p. We.8.C.3, 2010.

[119] J. Karout, X. Liu, S. Chandrasekhar, E. Agrell, M. Karlsson, and R.-J. Essiambre, "Experimental demonstration of an optimized 16-ary four-dimensional modulation format using optical OFDM," in *Optical Fiber Communication Conference (OFC)*, p. OW3B.4, 2013.

[120] H. Bülow, T. Rahman, F. Buchali, W. Idler, and W. Kuebart, "Transmission of 4-D modulation formats at 28-Gbaud," in *Optical Fiber Communication Conference (OFC)*, p. JW2A.39., 2013.

[121] S. Benedetto and P. Poggiolini, "Theory of polarization shift keying modulation," *IEEE Transactions on Communications*, vol. 40, no. 4, pp. 708–721, 1992.

[122] F. Buchali and H. Bülow, "Experimental transmission with POLQAM and PS-QPSK modulation format using a 28-Gbaud 4-D transmitter," in *European Conference and Exhibition on Optical Communication (ECOC)*, p. We.3.A.1, 2012.

[123] J. K. Fischer, S. Alreesh, R. Elschner, F. Frey, C. Meuer, L. Molle, C. Schmidt-Langhorst, T. Tanimura, and C. Schubert, "Experimental investigation of 126-Gb/s 6PolSK-QPSK signals," in *European Conference and Exhibition on Optical Communication (ECOC)*, vol. 2, p. We.1.C.4, 2012.

[124] M. Sjödin, E. Agrell, and M. Karlsson, "Subset-optimized polarization-multiplexed PSK for fiber-optic communications," *IEEE Communications Letters*, vol. 17, no. 5, pp. 838–840, 2013.

[125] T. Koike-Akino, D. S. Millar, K. Kojima, and K. Parsons, "Eight-dimensional modulation for coherent optical communications," in *European Conference and Exhibition on Optical Communication (ECOC)*, p. Tu.3.C.3, 2013.

[126] H. Bülow, H. Al-Hashimi, and B. Schmauss, "Coherent multimode-fiber MIMO transmission with spatial constellation modulation," in *European Conference and Exhibition on Optical Communication (ECOC)*, p. Tu.5.B.3, 2011.

[127] E. Agrell and M. Karlsson, "On the symbol error probability of regular polytopes," *IEEE Transactions on Information Theory*, vol. 57, no. 6, pp. 3411–3415, 2011.

[128] X. Liu, T. H. Wood, R. Tkach, and S. Chandrasekhar, "Demonstration of record sensitivity in an optically pre-amplified receiver by combining PDM-QPSK and 16-PPM with pilot-assisted digital coherent detection," in *Optical Fiber Communication Conference (OFC)*, p. PDPB1, 2011.

[129] M. Karlsson and E. Agrell, "Generalized pulse-position modulation for optical power-efficient communication," in *European Conference and Exhibition on Optical Communication (ECOC)*, p. Tu.6.B.6, 2011.

[130] H. Sugiyama and K. Nosu, "MPPM: a method for improving the band-utilization efficiency in optical PPM," *Journal of Lightwave Technology*, vol. 7, no. 3, pp. 465–472, 1989.

[131] J. Hamkins and B. Moision, "Multipulse pulse-position modulation on discrete memoryless channels," *Interplanetary Network Progress Report*, vol. 42, pp. 1–13, 2005.

[132] J. H. Nijhof, "Generalized L-out-of-K pulse position modulation for improved power efficiency and spectral efficiency," in *Optical Fiber Communication Conference (OFC)*, p. OW3H.7, 2012.

[133] H. Selmy, H. M. H. Shalaby, and Z.-I. Kawasaki, "Proposal and performance evaluation of a hybrid BPSK-modified MPPM technique for optical fiber communications systems," *Journal of Lightwave Technology*, vol. 31, no. 22, pp. 3535–3545, 2013.

[134] X. Liu, S. Chandrasekhar, T. H. Wood, R. W. Tkach, P. J. Winzer, E. C. Burrows, and A. R. Chraplyvy, "M-ary pulse-position modulation and frequency-shift keying with additional polarization/phase modulation for high-sensitivity optical transmission," *Optics Express*, vol. 19, no. 26, pp. B868–B881, 2011.

[135] W. Ryan and S. Lin, *Channel Codes: Classical and Modern.* Cambridge University Press, 2009.

[136] D. Caplan, B. Robinson, R. Murphy, and M. Stevens, "Demonstration of 2.5-Gslot/s optically-preamplified M-PPM with 4 photons/bit receiver sensitivity," in *Optical Fiber Communication Conference (OFC)*, p. PDP32, 2005.

[137] A. Ludwig, M.-L. Schulz, P. Schindler, R. Schmogrow, A. Mustafa, B. Moos, S. Brunsch, T. Dippon, D. Malsam, D. Hillerkuss, F. Roos, W. Freude, C. G. Koos, and J. Leuthold, "Stacking PS-QPSK and 64PPM for long-range free-space transmission," in *Signal Processing in Photonic Communication (SPPCom)*, p. NW2C.2, 2013.

[138] I. Fatadin, S. J. Savory, and D. Ives, "Compensation of quadrature imbalance in an optical QPSK coherent receiver," *IEEE Photonics Technology Letters*, vol. 20, no. 20, pp. 1733–1735, 2008.

[139] J. G. Aiken, J. A. Erdos, and J. A. Goldstein, "On Löwdin orthogonalization," *International Journal of Quantum Chemistry*, vol. 18, pp. 1101–1108, Oct. 1980.

[140] S. H. Chang, H. S. Chung, and K. Kim, "Impact of quadrature imbalance in optical coherent QPSK receiver," *IEEE Photonics Technology Letters*, vol. 21, no. 11, pp. 709–711, 2009.

[141] A. Matiss, M. Nölle, J. K. J. Fischer, C. C. Leonhardt, R. Ludwig, J. Hilt, L. Molle, C. Schmidt-Langhorst, and C. Schubert, "Characterization of an integrated coherent receiver for 224 Gb/s polarization multiplexed 16-QAM transmission," *Optical Fiber Communication Conference (OFC)*, p. JWA026, 2011.

[142] E. Ip and J. M. Kahn, "Digital equalization of chromatic dispersion and polarization mode dispersion," *Journal of Lightwave Technology*, vol. 25, no. 8, pp. 2033–2043, 2007.

[143] C. Fludger, T. Duthel, D. van den Borne, C. Schulien, E.-D. Schmidt, T. Wuth, J. Geyer, E. De Man, G.-D. Khoe, and H. de Waardt, "Coherent equalization and POLMUX-RZ-DQPSK for robust 100-GE transmission," *Journal of Lightwave Technology*, vol. 26, no. 1, pp. 64–72, 2008.

[144] G. Gavioli, E. Torrengo, G. Bosco, A. Carena, V. Curri, V. Miot, P. Poggiolini, F. Forghieri, S. J. Savory, L. Molle, and R. Freund, "NRZ-PM-QPSK 16 $\times$ 100 Gb/s transmission over installed fiber with different dispersion maps," *IEEE Photonics Technology Letters*, vol. 22, no. 6, pp. 371–373, 2010.

[145] M. S. Alfiad, D. van den Borne, T. Wuth, M. Kuschnerov, and H. de Waardt, "On the tolerance of 111-Gb/s POLMUX-RZ-DQPSK to nonlinear transmission effects," *Journal of Lightwave Technology*, vol. 29, no. 2, pp. 162–170, 2011.

[146] V. Sleiffer, D. van den Borne, M. Alfiad, S. Jansen, and H. de Waardt, "Dispersion management in long-haul 111-Gb/s POLMUX-RZ-DQPSK transmission systems," in *2009 IEEE LEOS Annual Meeting*, pp. 569–570, 2009.

[147] E. Tipsuwannakul, J. Li, T. A. Eriksson, L. Egnell, F. Sjöström, J. Pejnefors, P. A. Andrekson, and M. Karlsson, "Influence of fiber-bragg grating-induced group-delay ripple in high-speed transmission systems," *Journal of Optical Communications and Networking*, vol. 4, no. 6, pp. 514–521, 2012.

[148] S. J. Savory, "Digital filters for coherent optical receivers," *Optics Express*, vol. 16, no. 2, pp. 804–817, 2008.

[149] M. Kuschnerov, F. Hauske, K. Piyawanno, B. Spinnler, M. M. S. Alfiad, A. Napoli, and B. Lankl, "DSP for coherent single-carrier receivers," *Journal of Lightwave Technology*, vol. 27, no. 16, pp. 3614–3622, 2009.

[150] D. N. Godard, "Self-recovering equalization and carrier tracking in two-dimensional data communication systems," *IEEE Transactions on Communications*, vol. 28, no. 11, pp. 1867–1875, 1980.

[151] K. Kikuchi, "Polarization-demultiplexing algorithm in the digital coherent receiver," in *Digest 2008 IEEE/LEOS Summer Topical Meetings*, pp. 101–102, 2008.

[152] M. Kuschnerov, M. Chouayakh, K. Piyawanno, B. Spinnler, E. de Man, P. Kainzmaier, M. S. Alfiad, a. Napoli, and B. Lankl, "Data-aided versus blind single-carrier coherent receivers," *IEEE Photonics Journal*, vol. 2, no. 3, pp. 387–403, 2010.

[153] F. Pittalà, F. N. Hauske, Y. Ye, I. Tafur Monroy, and J. A. Nossek, "Training-based channel estimation for signal equalization and OPM in 16-QAM optical transmission systems," in *European Conference and Exhibition on Optical Communication (ECOC)*, p. P3.16, 2012.

[154] I. Fatadin, D. Ives, and S. J. Savory, "Blind equalization and carrier phase recovery in a 16-QAM optical coherent system," *Journal of Lightwave Technology*, vol. 27, no. 15, pp. 3042–3049, 2009.

[155] H. Louchet, K. Kuzmin, and A. Richter, "Improved DSP algorithms for coherent 16-QAM transmission," in *European Conference on Optical Communication (ECOC)*, p. Tu.1.E.6, 2008.

[156] M. J. Ready and R. P. Gooch, "Blind equalization based on radius directed adaptation," in *International Conference on Acoustics, Speech, and Signal Processing*, p. D11.16, 1990.

[157] P. Johannisson, H. Wymeersch, M. Sjödin, A. S. Tan, E. Agrell, P. A. Andrekson, and M. Karlsson, "Convergence comparison of the CMA and ICA for blind polarization demultiplexing," *Journal of Optical Communications and Networking*, vol. 3, no. 6, pp. 493–501, 2011.

[158] S. Hoffmann, S. Bhandare, T. Pfau, O. Adamczyk, C. Wordehoff, R. Peveling, M. Porrmann, and R. Noé, "Frequency and phase estimation for coherent QPSK transmission with unlocked DFB lasers," *IEEE Photonics Technology Letters*, vol. 20, no. 18, pp. 1569–1571, 2008.

[159] A. Leven, N. Kaneda, U.-V. Koc, and Y.-K. Chen, "Frequency estimation in intradyne reception," *IEEE Photonics Technology Letters*, vol. 19, no. 6, pp. 366–368, 2007.

[160] M. Seimetz, "Performance of coherent optical square-16-QAM-systems based on IQ-transmitters and homodyne receivers with digital phase estimation," in *Optical Fiber Communication Conference (OFC)*, p. NWA4, 2006.

[161] A. J. Viterbi and A. M. Viterbi, "Nonlinear estimation of PSK-modulated carrier phase with application to burst digital transmission," *IEEE Transactions on Information Theory*, vol. 29, no. 4, pp. 543–551, 1983.

[162] M. G. Taylor, "Phase estimation methods for optical coherent detection using digital signal processing," *Journal of Lightwave Technology*, vol. 27, no. 7, pp. 901–914, 2009.

[163] E. Ip and J. M. Kahn, "Feedforward carrier recovery for coherent optical communications," *Journal of Lightwave Technology*, vol. 25, no. 9, pp. 2675–2692, 2007.

[164] M. Kuschnerov, D. van den Borne, K. Piyawanno, F. Hauske, C. Fludger, T. Duthel, T. Wuth, J. Geyer, C. Schulien, B. Spinnler, E.-D. Schmidt, and B. Lankl, "Joint-polarization carrier phase estimation for XPM-limited coherent polarization-multiplexed QPSK transmission with OOK-neighbors," in *European Conference and Exhibition on Optical Communication (ECOC)*, p. Mo.4.D.2, 2008.

[165] S. Alreesh, J. K. Fischer, M. Nolle, and C. Schubert, "Joint-polarization carrier phase estimation for PS-QPSK signals," *IEEE Photonics Technology Letters*, vol. 24, no. 15, pp. 1282–1284, 2012.

[166] I. Fatadin, D. Ives, and S. J. Savory, "Laser linewidth tolerance for 16-QAM coherent optical systems using QPSK partitioning," *IEEE Photonics Technology Letters*, vol. 22, pp. 631–633, May 2010.

[167] R. W. Tkach, "Scaling optical communications for the next decade and beyond," *Bell Labs Technical Journal*, vol. 14, no. 4, pp. 3–9, 2010.

[168] D. J. Richardson, J. M. Fini, and L. E. Nelson, "Space-division multiplexing in optical fibres," *Nature Photonics*, vol. 7, no. 5, pp. 354–362, 2013.

[169] A. Ellis and N. Doran, "Are few-mode fibres a practical solution to the capacity crunch?," in *International Conference on Transparent Optical Networks (ICTON)*, p. Tu.C2.1, 2013.

[170] J. Sakaguchi, B. J. Puttnam, W. Klaus, Y. Awaji, N. Wada, A. Kanno, T. Kawanishi, K. Imamura, H. Inaba, K. Mukasa, R. Sugizaki, T. Kobayashi, and M. Watanabe, "19-core fiber transmission of 19x100x172-Gb/s SDM-WDM-PDM-QPSK signals at 305Tb/s," in *Optical Fiber Communication Conference (OFC)*, p. PDP5C.1, 2012.

[171] S. Randel, M. Magarini, R. Ryf, R.-J. Essiambre, A. H. Gnauck, and P. J. Winzer, "MIMO-based signal processing of spatially multiplexed 112-Gb/s PDM-QPSK signals using strongly-coupled 3-core fiber," in *European Conference and Exhibition on Optical Communication (ECOC)*, p. Tu.5.B.1., 2011.

[172] D. Qian, E. Ip, M.-F. Huang, M.-J. Li, A. Dogariu, S. Zhang, Y. Shao, Y.-K. Huang, Y. Zhang, X. Cheng, Y. Tian, P. Ji, A. Collier, Y. Geng, J. Linares, C. Montero, V. Moreno, X. Prieto, and T. Wang, "1.05Pb/s transmission with 109b/s/Hz spectral efficiency using hybrid single- and few-mode cores," in *Frontiers in Optics*, p. FW6C.3, 2012.

[173] S. Jain, T. May-Smith, V. Rancaño, P. Petropoulos, D. Richardson, and J. Sahu, "Multi-element fibre for space-division multiplexed transmission," in *European Conference and Exhibition on Optical Communication (ECOC)*, p. Mo.4.A.2, 2013.

[174] B. J. Puttnam, J. Sakaguchi, W. Klaus, Y. Awaji, J. M. Delgado Mendinueta, N. Wada, A. Kanno, and T. Kawanishi, "Investigating self-homodyne coherent detection in a 19-core spatial-division-multiplexed transmission link," in *European Conference and Exhibition on Optical Communication (ECOC)*, p. Tu.3.C.3, 2012.

[175] ITU-T, "Interfaces for the optical transport network," ITU-T G.709/Y.1331, 2012.